Article

Cancer Cell

A SIRT2-Selective Inhibitor Promotes c-Myc Oncoprotein Degradation and Exhibits Broad Anticancer Activity

Highlights

- TM, a SIRT2 inhibitor with excellent potency and specificity, has been developed
- TM has broad anticancer activity
- SIRT2 inhibition promotes c-Myc ubiquitination and degradation
- SIRT2 is a promising target for c-Myc-driven cancers

Authors

Hui Jing, Jing Hu, Bin He, ..., Paraskevi Giannakakou, Robert S. Weiss, Hening Lin

Correspondence

hl379@cornell.edu

In Brief

Jing et al. develop a thiomyristoyl lysine compound, TM, as a potent SIRT2-specific inhibitor with broad anticancer activity but little effect on non-cancerous cells. SIRT2 inhibition promotes c-Myc ubiquitination and degradation, suggesting the therapeutic potential of TM to target certain c-Myc-driven cancers.

Jing et al., 2016, Cancer Cell *29*, 297–310
March 14, 2016 ©2016 Elsevier Inc.
http://dx.doi.org/10.1016/j.ccell.2016.02.007

CellPress

Cancer Cell
Article

A SIRT2-Selective Inhibitor Promotes c-Myc Oncoprotein Degradation and Exhibits Broad Anticancer Activity

Hui Jing,[1] Jing Hu,[1] Bin He,[1,6] Yashira L. Negrón Abril,[2] Jack Stupinski,[2] Keren Weiser,[3] Marisa Carbonaro,[3] Ying-Ling Chiang,[1] Teresa Southard,[2] Paraskevi Giannakakou,[3,5] Robert S. Weiss,[2,5] and Hening Lin[1,4,5,*]
[1]Department of Chemistry and Chemical Biology
[2]Department of Biomedical Sciences
Cornell University, Ithaca, NY 14853, USA
[3]Division of Hematology & Medical Oncology, Weill Medical College of Cornell University, 1300 York Avenue, C610C, New York, NY 10065-4896, USA
[4]Howard Hughes Medical Institute, Department of Chemistry and Chemical Biology, Cornell University, Ithaca, NY 14853, USA
[5]Co-senior author
[6]Present address: School of Pharmacy, Guizhou Medical University, Guiyang 550004, Guizhou, China
*Correspondence: hl379@cornell.edu
http://dx.doi.org/10.1016/j.ccell.2016.02.007

SUMMARY

Targeting sirtuins for cancer treatment has been a topic of debate due to conflicting reports and lack of potent and specific inhibitors. We have developed a thiomyristoyl lysine compound, TM, as a potent SIRT2-specific inhibitor with a broad anticancer effect in various human cancer cells and mouse models of breast cancer. Mechanistically, SIRT2 inhibition promotes c-Myc ubiquitination and degradation. The anticancer effect of TM correlates with its ability to decrease c-Myc level. TM had limited effects on non-cancerous cells and tumor-free mice, suggesting that cancer cells have an increased dependency on SIRT2 that can be exploited for therapeutic benefit. Our studies demonstrate that SIRT2-selective inhibitors are promising anticancer agents and may represent a general strategy to target certain c-Myc-driven cancers.

INTRODUCTION

Oncogenes that drive tumorigenesis have attracted extensive interest as therapeutic targets for treating cancers. *MYC*, and *c-Myc* in particular, is one such oncogene. *MYC* was discovered in studies of fulminant chicken tumors caused by oncogenic retroviruses, which co-opted cellular c-Myc to generate the oncogenic v-Myc (Meyer and Penn, 2008). Subsequently, mouse plasmacytomas and human Burkitt lymphomas were found to be caused by *c-Myc* activation due to chromosomal translocations that fused *c-Myc* to the immunoglobulin gene loci (Meyer and Penn, 2008). Recent genomic sequencing efforts identified *c-Myc* as one of the most highly amplified oncogenes in many different human cancers, further highlighting the oncogenic role of c-Myc activation (Beroukhim et al., 2010). The identification of effective therapeutic strategies targeting Myc has been challenging. Recently it was demonstrated that bromodomain inhibitors that target BRD4 could suppress *c-Myc* transcription and lead to tumor inhibition in vivo (Delmore et al., 2011). This finding underscores the therapeutic value of targeting Myc.

The sirtuin family of NAD-dependent protein lysine deacylases has been shown to play important roles in many physiological processes, including the regulation of transcription, metabolism, and DNA repair (Haigis and Sinclair, 2010; Imai et al., 2000; Imai and Guarente, 2010). Many of these functions are achieved by their ability to deacylate various substrate proteins, including histones, transcription factors, and metabolic enzymes (Du et al., 2011; Haigis and Sinclair, 2010; Imai et al., 2000; Imai and

Significance

Inhibiting oncoproteins frequently found in cancers is a common theme in targeted cancer therapy. One such oncoprotein is c-Myc, which is up-regulated in ~50% of human tumors. Small molecules targeting c-Myc are highly sought as anticancer agents. Our studies identified SIRT2 as a promising target to treat c-Myc-driven cancers. We have developed a SIRT2 inhibitor with the best combination of potency and selectivity reported, and show that it has broad anticancer activity with little effect on non-cancerous cells. The small-molecule inhibitor studies combined with knockdown and/or overexpression of sirtuins provide extensive evidence establishing SIRT2 as a promising anticancer target, especially for certain c-Myc-driven cancers.

Guarente, 2010; Jiang et al., 2013; Peng et al., 2011; Zhu et al., 2012). Because the functionally related but structurally distinct zinc-dependent histone deacetylases (HDACs) are established cancer targets (Lee et al., 2012; Marks and Breslow, 2007), there is interest in exploring whether sirtuins can also be important targets for cancers (Fang and Nicholl, 2011; Herranz and Serrano, 2010; Stünkel and Campbell, 2011). However, there is evidence suggesting both tumor-suppressor and oncogenic roles of sirtuins (Fang and Nicholl, 2011; Herranz and Serrano, 2010; Stünkel and Campbell, 2011). In the case of SIRT2, genetic studies indicated that aged *Sirt2* knockout (KO) mice show increased tumor incidence compared with wild-type (WT) (Kim et al., 2011a) controls. In contrast, SIRT2 was also observed to have tumor-promoting activity in several studies (Chen et al., 2013; Liu et al., 2013; McGlynn et al., 2014; Soung et al., 2014; Yang et al., 2013; Zhao et al., 2013, 2014). Moreover, several SIRT2 inhibitors have also been reported to have anticancer effects (Cheon et al., 2015; He et al., 2014; Heltweg et al., 2006; Hoffmann et al., 2014; Kim et al., 2011b; Mahajan et al., 2014; McCarthy et al., 2013; Neugebauer et al., 2008; Rotili et al., 2012; Zhang et al., 2009). However, the moderate potency and specificity of the existing sirtuin inhibitors are insufficient to draw conclusions about the anticancer potential of sirtuin inhibition. Thus, whether sirtuin inhibitors are useful anticancer agents is still an open question. Here, we set out to develop sirtuin inhibitors with improved potency and selectivity to explore the potential of targeting sirtuins for treating human cancers, especially c-Myc-driven cancers.

RESULTS

Development of a Highly Selective and Potent SIRT2 Inhibitor

Most existing sirtuin inhibitors are either not very potent (e.g., with IC_{50} values in the high micromolar range) or not very selective (i.e., they inhibit several different sirtuins). More potent and more selective sirtuin inhibitors would greatly aid in evaluating the therapeutic potential of targeting sirtuins. To develop potent inhibitors specific for a particular sirtuin, we used mechanism-based thioacyl lysine compounds. Thioacyl lysine peptides can react with NAD in the sirtuin active site, forming a relatively stable intermediate that inhibits sirtuin (Figure 1A) (Fatkins et al., 2006; Hawse et al., 2008; Smith and Denu, 2007). Recent studies suggested that different sirtuins may have different acyl group specificity (Du et al., 2011; Feldman et al., 2013; Jiang et al., 2013; Zhu et al., 2012), which can be utilized to design inhibitors specific for different sirtuins (He et al., 2012, 2014). To target the sirtuins that can recognize aliphatic acyl groups, we synthesized four thioacyl lysine compounds, TA (thioacetyl) (Suzuki et al., 2009), TB (thiobutyryl), TH (thioheptanoyl), and TM (thiomyristoyl) (Figure 1B), and analyzed their ability to inhibit different sirtuins.

Remarkable differences in the potency and selectivity of these compounds were observed by sirtuin activity assays in vitro (Figures 1C and S1A). TA could inhibit SIRT1, SIRT2, and SIRT3, but not very potently. TB was a better SIRT1/SIRT2 inhibitor than TA. The IC_{50} values of TB for SIRT1 (3.8 μM) and SIRT2 (0.43 μM) were about 3-fold and >10-fold, respectively, better than those of TA (Figure 1C). Further increasing the size of the thioacyl group by three methylene groups led to TH, which had even lower IC_{50} values for SIRT1 (1.2 μM) and SIRT2 (0.13 μM). Remarkably, TM, with a 14-carbon thioacyl group, could inhibit SIRT2 with an IC_{50} value of 0.028 μM, but inhibited SIRT1 with an IC_{50} value of 98 μM and did not inhibit SIRT3 even at 200 μM (Figure 1C). None of these compounds can efficiently inhibit SIRT5, SIRT6, or SIRT7. Thus, TM is a SIRT2-speific inhibitor in vitro. To facilitate later investigations of TM, we also synthesized the corresponding myristoyl lysine compound (M, Figure 1B) as an inactive control for TM. M differs from TM by only one atom (the S atom in TM is changed to an O atom in M). As expected, M did not show sirtuin inhibition even at 200 μM (Figure 1C).

To further confirm that TM is a mechanism-based inhibitor of SIRT2, we performed substrate competition analyses for TM-mediated SIRT2 inhibition. At saturating NAD concentration, the apparent K_m value for acetyl-H3K9 peptide (acH3K9) increased with increasing TM concentrations, whereas the v_{max} remained relatively constant (Figure 1E). The double-reciprocal plot of $1/v$ versus 1/[acH3K9] revealed a series of lines that intersect at the $1/v$ axis (Figure S1C), suggesting that TM is competitive with acH3K9. This is consistent with our recent finding that SIRT2 possesses a large hydrophobic pocket that can accommodate the myristoyl group (Teng et al., 2015). At saturating acH3K9 concentration, both the apparent K_m value for NAD and v_{max} decreased with increasing TM concentrations (Figure 1F), suggesting that TM is uncompetitive with NAD, which is consistent with the fact that formation of the inhibitory covalent intermediate requires NAD. We then used liquid chromatography-mass spectrometry to examine the formation of the stalled covalent intermediate. Ions with m/z of 1,123.33 (the protonated intermediate) and 1,145.25 (the sodium adduct of the intermediate) were detected only when TM was incubated with both SIRT2 and NAD (Figure 1D), but not without SIRT2 or NAD (Figure S1B). Overall, these results indicate that TM acts as a mechanism-based inhibitor of SIRT2.

TM Exhibits Potent Anticancer Activity

Sirtuin inhibitors have been reported to have anticancer properties. However, most of the inhibitors used are not very selective and, thus, inhibiting which sirtuins can provide beneficial effects remains unclear. Having a potent and very selective SIRT2 inhibitor provided a unique opportunity to investigate whether inhibiting SIRT2 can be useful as an anticancer strategy. We initially explored this in several breast cancer cell lines because of the substantial tumor-promoting role of SIRT2 in breast cancer (McGlynn et al., 2014; Soung et al., 2014; Zhao et al., 2014) and the previous studies showing that SIRT2 inhibitors exert an antiproliferative effect against breast cancer cell lines (Di Fruscia et al., 2012; Neugebauer et al., 2008; Rotili et al., 2012; Seifert et al., 2014; Yoon et al., 2014). We assayed the ability of TA, TB, TH, and TM to inhibit three human breast cancer cell lines, MCF-7, MDA-MB-468, and MDA-MB-231. The cytotoxicity of these compounds correlated with their in vitro SIRT2 inhibitory effects (Figures 2A and S2A). TA, which showed modest SIRT1, SIRT2, and SIRT3 inhibition in vitro, did not inhibit cell viability at 50 μM. TB had greater inhibitory effect on cell viability than TA, but only showed inhibition at 50 μM. TH and TM were more potent than TA and TB. Compared with TH, the

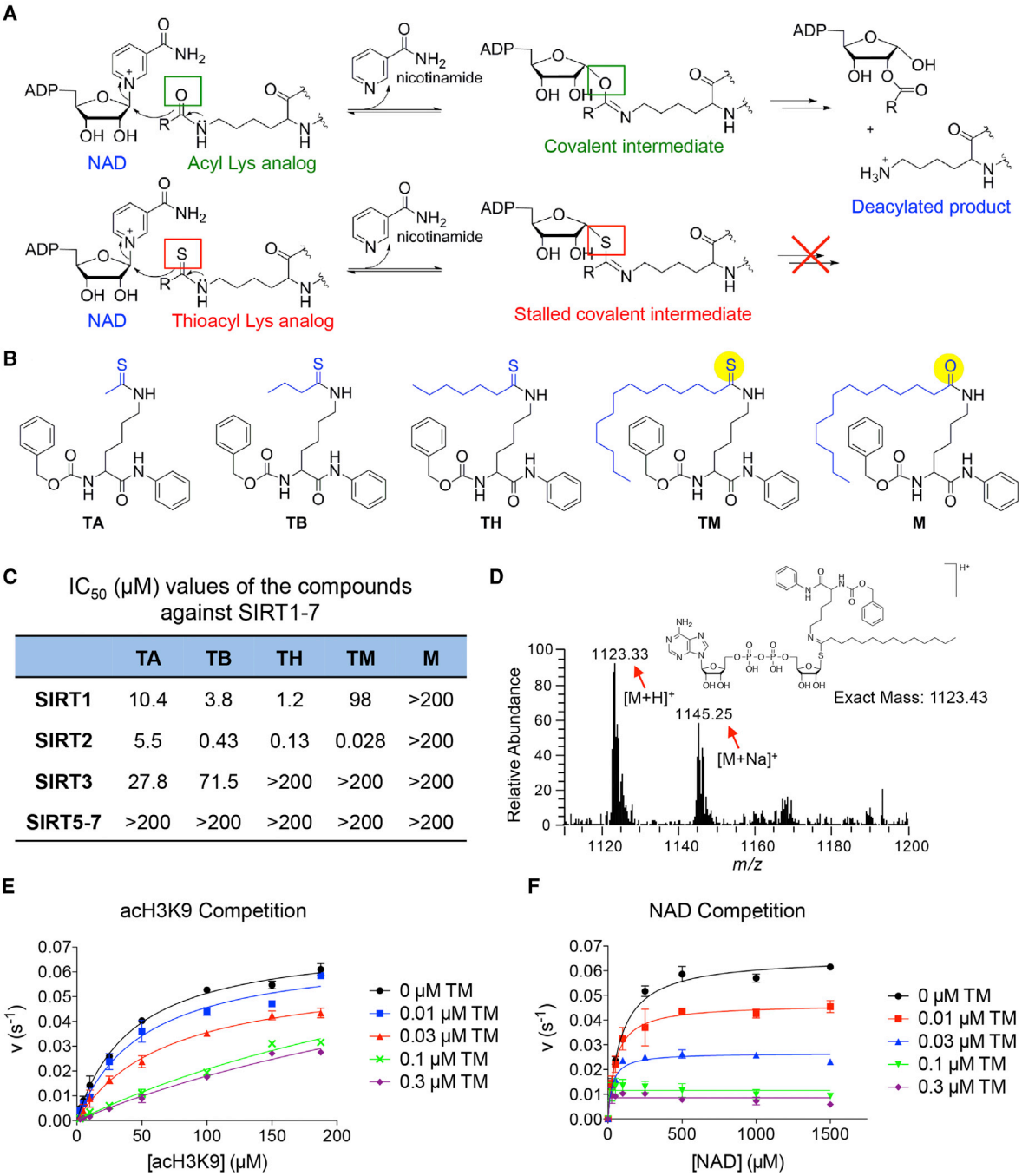

	TA	TB	TH	TM	M
SIRT1	10.4	3.8	1.2	98	>200
SIRT2	5.5	0.43	0.13	0.028	>200
SIRT3	27.8	71.5	>200	>200	>200
SIRT5-7	>200	>200	>200	>200	>200

Figure 1. Development of Mechanism-Based Inhibitor of Sirtuins

(A) The enzymatic reaction mechanism of sirtuin-catalyzed NAD-dependent deacylation (upper panel). Thioacyl lysine compounds act as suicide substrates to inhibit sirtuins (lower panel).

(B) Structures of four different thioacyl lysine sirtuin inhibitors, TA, TB, TH, and TM. M, which differs from TM by just one atom (highlighted by yellow color), is an inactive control of TM.

(C) IC_{50} (μM) values of TA, TB, TH, TM, and M against SIRT1-7. IC_{50} values derived from GraphPad Prism are presented as mean values from three independent experiments.

(D) Mass spectrometry detection of the stable covalent intermediate formed by TM and NAD.

(E and F) Henri-Michaelis-Menten plots showing acH3K9 (E) and NAD (F) competition analyses of TM-mediated SIRT2 inhibition.

Error bars represent mean ± SD. See also Figure S1.

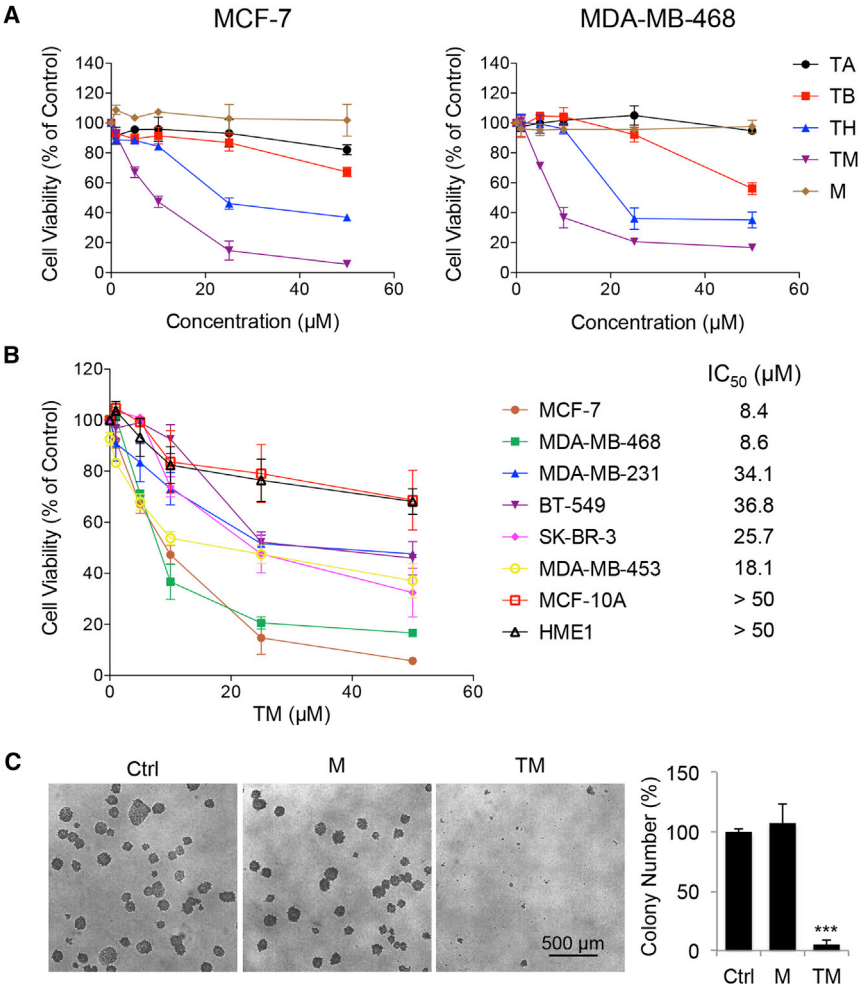

Figure 2. TM Inhibits Human Cancer Cells

(A) Cell viability of MCF-7 and MDA-MB-468 cells treated with the indicated inhibitors for 72 hr.

(B) Cell viability of the indicated human normal and breast cancer cells treated with TM for 72 hr. IC_{50} values were means from three independent experiments.

(C) Soft agar colony formation of MCF-7 cells treated with ethanol, TM (25 μM in ethanol), or M (25 μM in ethanol). Representative images of colonies are shown on the left panels. Quantification of the colony numbers is shown on the rightmost panel. The y axis represents percent colony number relative to ethanol-treated cells.

Statistical evaluation by two-tailed Student's t test. Error bars represent mean ± SD. ***$p < 0.001$. See also Figure S2.

SIRT2-selective inhibitor TM showed greater inhibition of cell viability. The inactive inhibitor mimic M did not affect cell viability at 50 μM. A similar result was also obtained in HeLa cells (Figure S2B). Next, we treated eight different human normal and breast cancer cell lines with TM. As shown in Figure 2B, different malignant cells showed differential susceptibility to TM. The two non-cancerous cell lines, MCF-10A and HME1, were much less sensitive to TM, suggesting that the cytotoxicity of TM is relatively selective toward cancer cells. We further evaluated the anticancer activity of TM using soft agar colony formation assay. TM significantly inhibited anchorage-independent growth of various cancer cells tested (Figures 2C and S2C), while the control compound M did not (Figure 2C).

The correlation between the cytotoxic effects of TA, TB, TH, TM, and M and their in vitro SIRT2 inhibitory activities suggests that SIRT2 inhibition could have anticancer effects. To further confirm this, we knocked down all seven sirtuins individually in MCF-7, MDA-MB-468, and HeLa cells, which were relatively sensitive to TM (Figure S3A). *SIRT2* knockdown (*SIRT2* KD) produced the strongest cytotoxicity in all three cell lines tested (Figures 3A and S3B), which further supported SIRT2 inhibition as a promising anticancer strategy.

We then further examined the effect of SIRT2 KD in the same set of human breast cancer and non-tumorigenic mammary cell lines in which the cytotoxic effect of TM was tested. SIRT2 KD significantly decreased cell viability in a time-dependent manner in MCF-7, MDA-MB-468, and MDA-MB-231 cells, but did not show much cytotoxicity in BT-549, SK-BR-3, and MDA-MB-453 cells or the non-transformed MCF-10A and HME1 cells (Figure 3B). In MCF-7 and MDA-MB-468 cells, SIRT2 KD resulted in less than 1% cell viability after 10 days of lentiviral infection (Figure S3C). Moreover, colony formation in soft agar by MCF-7 cells was dramatically diminished by *SIRT2* KD (Figures 3D–3F). The knockdown data are thus consistent with the small-molecule data, indicating that SIRT2 inhibition can effectively suppress cancer cell proliferation and that the anticancer effect of TM is likely through SIRT2 inhibition.

TM Inhibits SIRT2 in Cells

We next wanted to determine whether TM inhibits cancer cells by targeting SIRT2. We first carried out a number of experiments to validate that SIRT2 is the target of TM in cells. We conjugated biotin to TM and M to generate Biotin-TM and Biotin-M compounds (Figure S4A). We then added these compounds to either total protein extract (Figure 4A) or live cells (Figure 4B) to pull down sirtuins. Biotin-TM was able to pull down SIRT2 but not SIRT1 from the HEK293T cell extract. In contrast, Biotin-M, the inactive control compound, did not pull out SIRT2 (Figure 4A). When assayed using SIRT2 KD cells, the amount of SIRT2 pulled down by Biotin-TM was also decreased (Figure 4B). These data suggest that TM targets SIRT2 but not SIRT1 in cells.

Second, we confirmed that TM inhibits SIRT2 in cells by detecting the acetylation level of known SIRT2 as well as SIRT1 targets. In MCF-7 and MDA-MB-468 cells, TA, TB, and TH inhibited SIRT1, based on the acetylation level of a known SIRT1 deacetylation target, p53 (Figure 4D). In contrast, TM showed almost no inhibition of p53 deacetylation. By detecting the

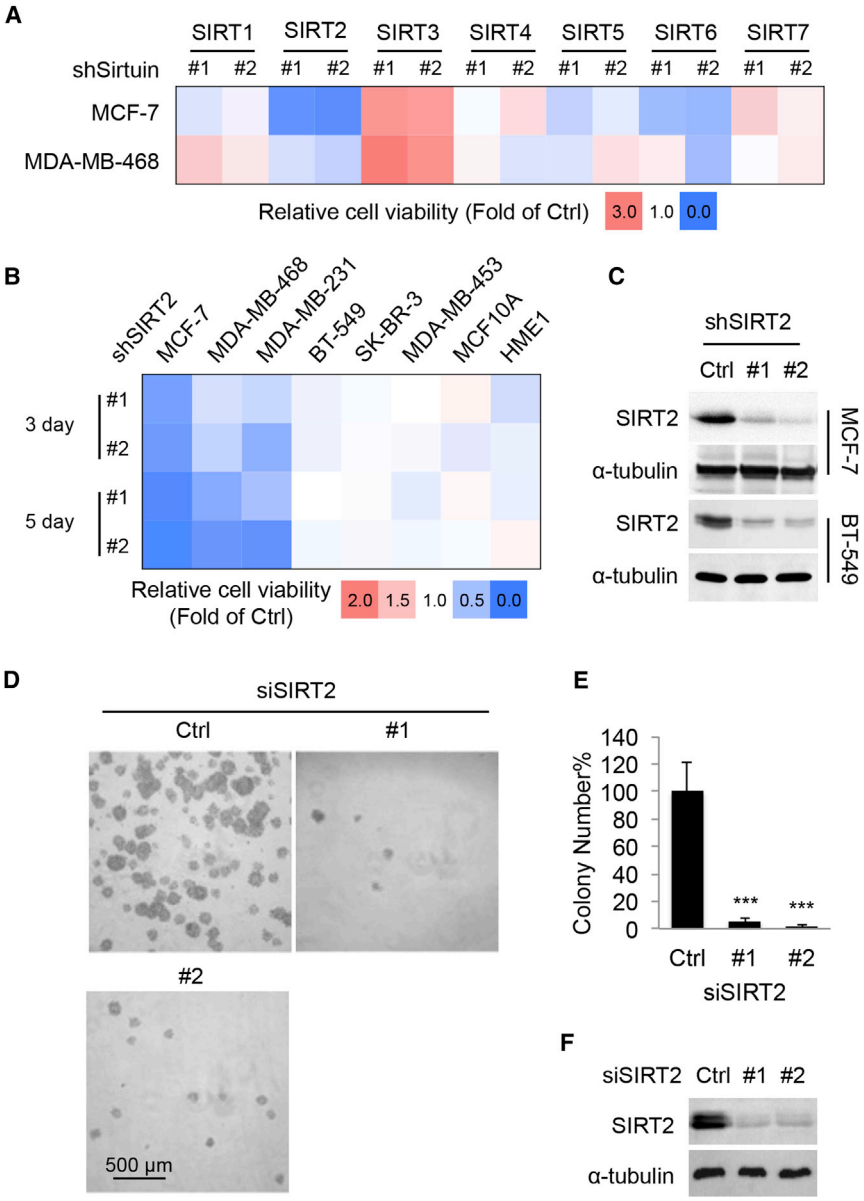

Figure 3. SIRT2 KD Decreases the Viability of Various Cancer Cell Lines

(A) Cell viability of MCF-7 and MDA-MB-468 cells infected with lentivirus carrying luciferase small hairpin RNA (shRNA) (Ctrl) or SIRT1-7 shRNAs for 72 hr. The heatmap presents average relative cell viability compared with Ctrl shRNA-infected cells from three independent experiments.

(B) Cell viability of various human normal and breast cancer cells infected with lentivirus carrying luciferase (Ctrl) or SIRT2 shRNAs.

(C) Representative western blots showing the knockdown efficiency of SIRT2 in MCF-7 and BT-549 cells.

(D) Soft agar colony formation of MCF-7 cells transfected with scrambled small interfering RNA (siRNA) or SIRT2 siRNA.

(E) Quantification of the colony numbers in (D). The y axis represents percent colony number relative to scrambled siRNA-transfected cells. Statistical evaluation by two-tailed Student's t test. Error bars represent mean ± SD. ***$p < 0.001$.

(F) Representative western blots showing the knockdown efficiency of SIRT2 by siRNAs in MCF-7 cells.

See also Figure S3.

acetylation of α-tubulin, a known SIRT2 target, we monitored SIRT2 inhibition. TA or M, which did not inhibit SIRT2 well, did not affect the acetylation of α-tubulin. TB and TH, which have intermediate SIRT2 inhibition potency, slightly increased the acetylation of α-tubulin. TM, the best SIRT2 inhibitor, led to the greatest increase in α-tubulin acetylation (Figure 4C). The effect of TM on α-tubulin acetylation was dose dependent, whereas M did not affect acetyl-α-tubulin level at 50 μM (Figure 4E). Similarly, TM, but not M, increased the level of α-tubulin acetylation in MDA-MB-231 cells based on immunofluorescence imaging (Figure 4F). SIRT2 has been reported to be not only a deacetylase but also a defatty-acylase (He et al., 2014; Liu et al., 2014), so we further examined the effect of TM on the defatty-acylase activity of SIRT2 in cells. Metabolic labeling of fatty-acylated proteins revealed that SIRT2 KD (Figure S4B), but not TM (Figure S4C), was able to elevate the fatty-acylation levels of many proteins, suggesting that in cells TM is a potent inhibitor of SIRT2 deacetylase but not defatty-acylase.

Finally, to confirm that the anticancer effect of TM is due to SIRT2 inhibition, we tested the sensitivity of cells to TM under SIRT2 overexpression or knockdown conditions. If TM inhibits cancer cells by targeting SIRT2, overexpression of SIRT2 would decrease the sensitivity of cells to TM (the increased SIRT2 level would require more TM for inhibition), while partial and transient knockdown of SIRT2 would increase the sensitivity. Indeed, overexpression of SIRT2 (Figure 4H) significantly decreased the cytotoxicity of TM (Figure 4G), while transient and partial knockdown of SIRT2 (Figure S4E) sensitized cells to TM (Figure S4D). These results support the conclusion that the anticancer effect of TM is through SIRT2 inhibition instead of other off-target effects.

TM Inhibits Tumor Growth in Mouse Models of Breast Cancer

To further demonstrate that SIRT2 inhibition can be useful for treating cancers, we tested TM in two mouse models of cancer. The first was a xenograft model in which the triple-negative breast cancer cell line, MDA-MB-231, was injected subcutaneously into immunocompromised mice. When tumor size reached ~200 mm^3, the mice were divided into two groups and treated by either direct intratumor (IT) (Figure S5) or intraperitoneal (IP) (Figure 5) injection of the control vehicle solvent

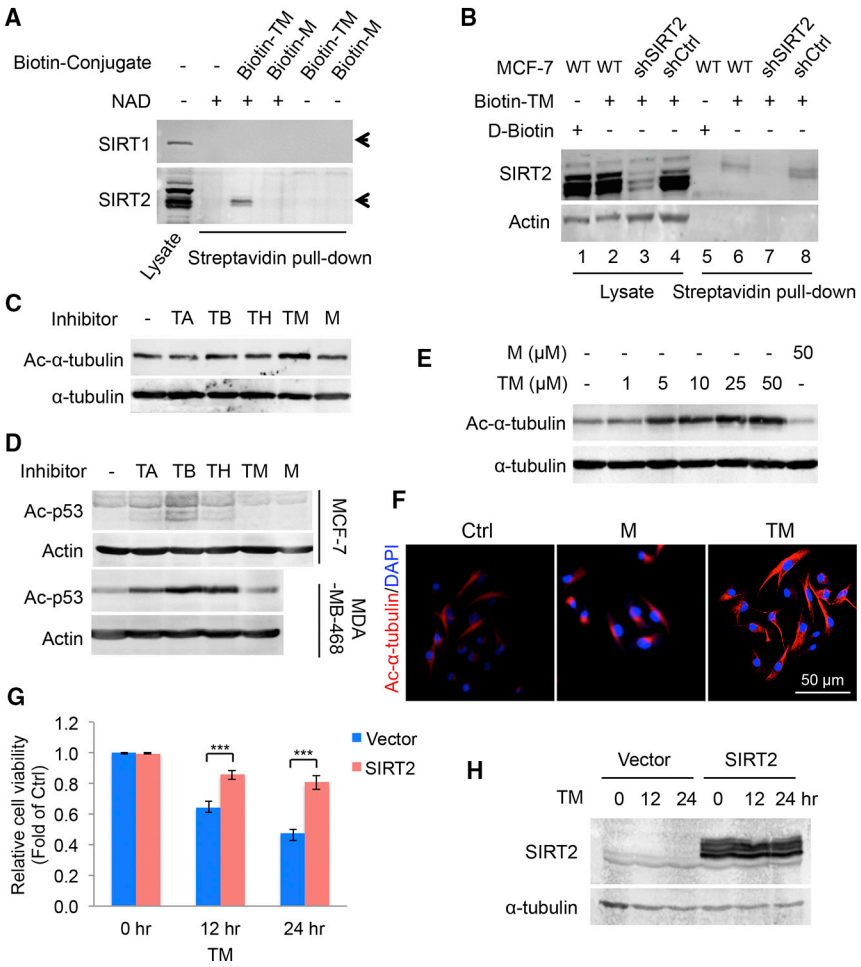

Figure 4. TM Specifically Inhibits SIRT2 in Cells

(A) Pull-down assay to detect the binding of Biotin-M (10 μM) and Biotin-TM (10 μM) to SIRT1 and SIRT2 in HEK293T total cell lysate.

(B) Pull-down assay to detect the binding of Biotin-TM (50 μM) to SIRT2 in MCF-7 cells. D-Biotin (50 μM) was used as a negative control.

(C) Immunoblot for the acetyl-α-tubulin (K40) levels in SIRT2-overexpressing MCF-7 cells treated with indicated inhibitors (25 μM) for 6 hr.

(D) Immunoblot for the acetylation of p53 (K382) in MCF-7 or MDA-MB-468 cells treated with TSA (200 nM) and the indicated inhibitors (25 μM) for 6 hr.

(E) Immunoblot for acetyl-α-tubulin (K40) levels in MCF-7 cells treated with TM or M for 6 hr.

(F) Immunofluorescence detection of the acetyl-α-tubulin (K40) level in MDA-MB-231 cells treated with ethanol, M, or TM (25 μM in ethanol) for 6 hr.

(G) Effect of SIRT2 overexpression on the cytotoxicity effect of TM. MCF-7 cells were transfected with pCMV vector or pCMV-*SIRT2* for 12 hr before being treated with 25 μM of TM for 12 or 24 hr. The y axis represents relative cell viability compared with ethanol-treated controls. Statistical evaluation by two-tailed Student's t test. Error bars represent mean ± SD. ***$p < 0.001$.

(H) SIRT2 overexpression in (G) was confirmed by western blot. See also Figure S4.

(DMSO) or TM (1.5 mg TM in 50 μl DMSO; n = 5) daily. Tumors were collected after 30 days of treatment and analyzed. TM treatment significantly inhibited tumor growth compared with the control (Figures S5A, S5B, and 5A). Histopathological examination revealed central areas of necrosis in tumors from both DMSO- and TM-treated mice, but the necrosis was more extensive and the overall tumor size was smaller in the TM-treated mice (Figures S5D and 5C). IT TM injection showed a stronger effect in reducing tumor volume and increasing areas of necrosis compared with IP TM injection. Analysis of TM content in tissue samples from TM-treated mice showed that IP-administered TM reached the tumors, even though the serum concentration of TM was low and a significant amount of TM accumulated in abdominal fat (Figure 5D). TM did not cause significant toxicity in mice (one mouse from each treatment group died, likely due to infection caused by repeated IP injection but not due to TM toxicity) and no significant weight loss was observed in TM-treated mice (Figures S5C and 5B). Immunohistochemical staining of Ki-67 was performed to assess the effect of TM on the proliferation of tumor cells in vivo. As shown in Figures 5E (upper panel) and 5F, as well as Figures S5F (upper panel) and S5G, a significant decrease in Ki-67$^+$ cells was observed with TM treatment relative to vehicle treatment. To determine whether TM inhibits SIRT2 in vivo, we performed immunofluorescence staining of acetyl-α-tubulin in the xenograft tumors. As shown in Figures 5E (lower panel) and 5G, and Figures S5F (lower panel) and S5H, the acetyl-α-tubulin level was moderately but statistically significantly increased in tumors from TM-treated mice compared with those from vehicle-treated mice, suggesting that TM indeed inhibits SIRT2 in vivo.

The second mouse model was the mammary tumor model driven by mammary gland-specific expression of polyoma middle T antigen under the control of mouse mammary tumor virus promoter/enhancer (MMTV-*PyMT* model) (Guy et al., 1992). The MMTV-*PyMT* mice received daily IP injections with either the control vehicle solvent (DMSO) or TM (1.5 mg TM in 50 μl of DMSO; n = 10). The Kaplan-Meier tumor-free survival curve showed that TM treatment significantly prolonged the tumor-free survival of mice compared with vehicle-treated mice (Figure 6A). While the average time to tumor onset in the control group was 48 days, the mean latency for TM-treated mice was 54 days. Histopathological examination revealed more extensive areas of necrosis in the neoplasms from TM-treated mice compared with the control group (Figure 6B). A significant decrease in proliferation of tumor cells was observed with TM treatment relative to vehicle treatment as measured by Ki-67 staining (Figures 6C [upper panel] and 6D). A modest but statistically significant increase in the acetyl-α-tubulin level was observed in tumors from TM-treated mice compared with those from vehicle-treated mice (Figures 6C [lower panel] and 6E), indicating that SIRT2 was inhibited by TM in vivo. These data demonstrate that SIRT2 inhibition with TM delays tumor

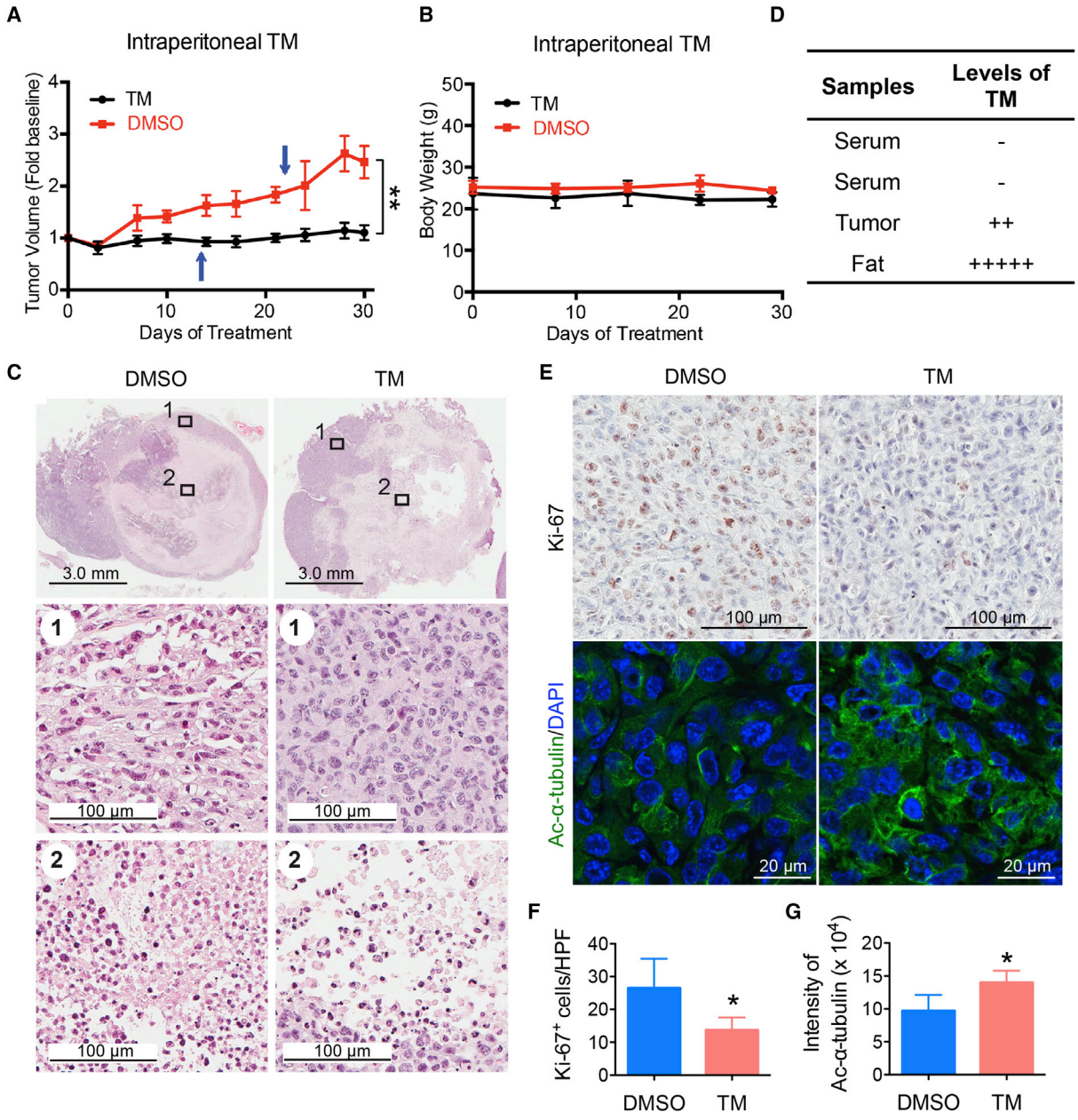

Figure 5. Analysis of Tumor Growth and Histopathological Findings of Xenografted Mice Treated by Intraperitoneal TM Injection

Mice bearing MDA-MB-231 human breast cancer xenograft were divided into two groups and treated by intraperitoneal injection with either the vehicle (DMSO) or TM (1.5 mg TM in 50 μl DMSO; n = 5) daily. Tumors were collected after 30 days of treatment.

(A) Tumor growth chart. Arrows indicate time point when an animal was found dead (one untreated, one treated). Statistical evaluation by paired Student's t test.

(B) Mouse body weight chart. Statistical evaluation by paired Student's t test.

(C) H&E staining of tumor tissues after 30 days of treatment with DMSO or TM. Lower four panels are the zoom-in images of the rectangles in the top two panels.

(D) Detection of TM in mouse serum, fat, and tumor tissues by mass spectrometry.

(E) Representative images of Ki-67 immunohistochemical staining and acetyl-α-tubulin (K40) immunofluorescence staining of tumor tissues after 30 days of treatment with DMSO or TM.

(F) Quantification of Ki-67$^+$ cells in (E). The y axis represents Ki-67$^+$ cells per high-power field (HPF) (10 HPFs/tumor for all the tumors analyzed, n = 3 for DMSO, n = 4 for TM). Statistical evaluation by unpaired Student's t test.

(G) Quantification of acetyl-α-tubulin fluorescence intensity in (E) by ImageJ. The y axis represents integrated intensity per cell (10 HPFs/tumor for all the tumors analyzed, n = 3 for DMSO, n = 4 for TM). Statistical evaluation by unpaired Student's t test.

Error bars represent mean ± SD. *$p < 0.05$, **$p < 0.01$. See also Figure S5.

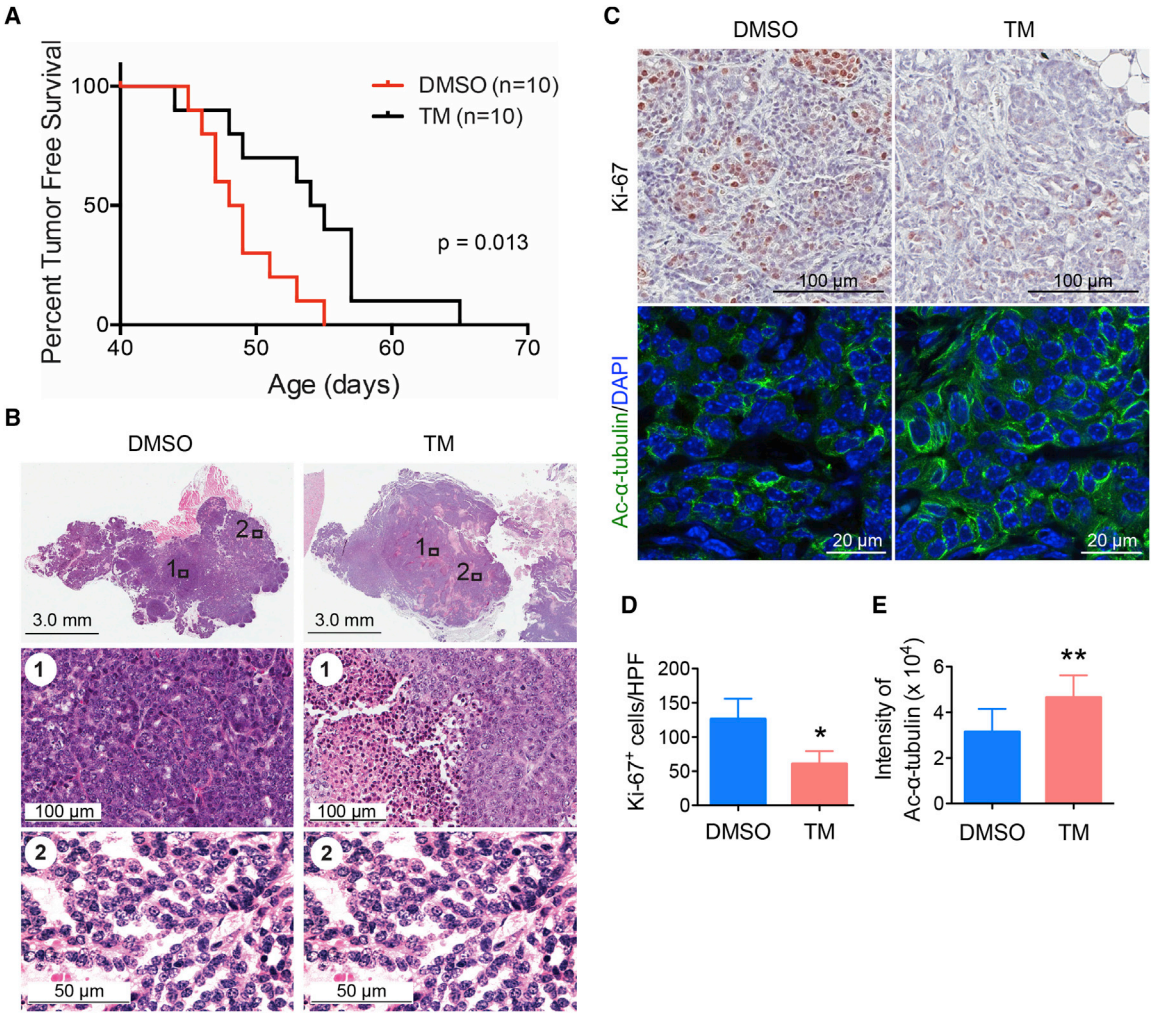

Figure 6. Mammary Tumorigenesis in MMTV-*PyMT* Female Mice following Intraperitoneal TM Injection

(A) Kaplan-Meier tumor-free survival curve of MMTV-*PyMT* mice treated by intraperitoneal injection with either the vehicle (DMSO) or TM (1.5 mg TM in 50 μl of DMSO; n = 10) daily. The x axis shows mouse age; the y axis shows proportion of mice remaining tumor free. Statistical evaluation by log-rank test.

(B) H&E staining of mammary tumors after 30 days of treatment with either DMSO or TM. Lower four panels are the zoom-in images of the rectangles in the top two panels.

(C) Representative images of Ki-67 immunohistochemical staining and acetyl-α-tubulin (K40) immunofluorescence staining of tumor tissues after 30 days of treatment with either DMSO or TM.

(D) Quantification of Ki-67$^+$ cells in (C). The y axis shows Ki-67$^+$ cells per HPF (10 HPFs/tumor for all the tumors analyzed, n = 4 for DMSO, n = 4 for TM). Statistical evaluation by unpaired Student's t test.

(E) Quantification of acetyl-α-tubulin fluorescence intensity in (C) by ImageJ. The y axis shows integrated intensity per cell (10 HPFs/tumor for all the tumors analyzed, n = 8 for DMSO, n = 8 for TM). Statistical evaluation by unpaired Student's t test.

Error bars represent mean ± SD. *$p < 0.05$, **$p < 0.01$.

onset in the MMTV-*PyMT* model and reduces tumor growth in vivo.

COMPARE Analysis with the NCI-60 Cancer Cell Panel Points to Possible Mechanism of Action for the SIRT2 Inhibitor TM

To further investigate the anticancer effects of TM, we first examined whether the level of SIRT2 in different cell lines could be used to predict which cell lines would be more sensitive to SIRT2 inhibitors. We checked the SIRT2 protein level in all of the eight human normal and breast cancer cell lines above (Figures 2B and 3B) to see whether the sensitivity to TM correlated with SIRT2 level in these cell lines. Compared with MCF-10A and HME1 cells, the cancer cell lines showed relatively high SIRT2 expression. However, we did not see an obvious correlation between SIRT2 level and TM sensitivity (Figures S6A and S6B) among the cancer cell lines, suggesting that other factors account for the SIRT2 inhibitor sensitivity.

To examine the anticancer activity of TM against other malignancies and the molecular mechanisms underlying its activity,

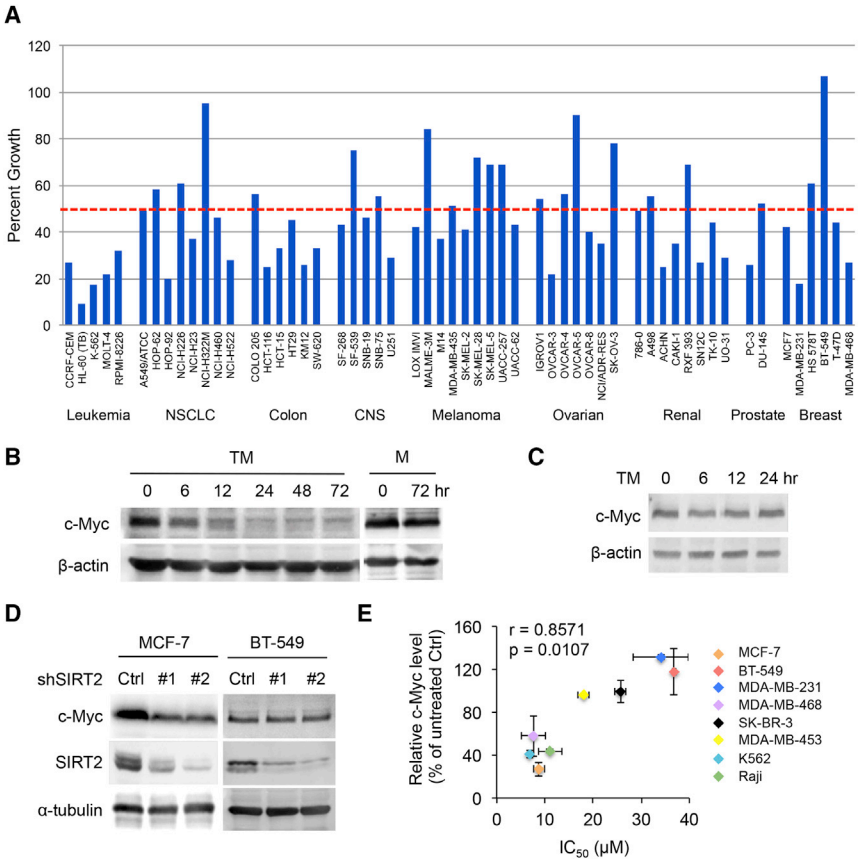

Figure 7. TM Inhibits Various Types of Human Cancer Cell Lines and Decreases c-Myc Protein Level

(A) NCI-60 cell line screening of TM. NCI-60 cell lines were cultured with and without 10 μM TM for 24 hr. The percent growth of TM-treated cells compared with the controls is shown. The horizontal dotted red line shows 50% growth.

(B) The c-Myc protein levels in MCF-7 cells treated with TM (25 μM) or M (25 μM).

(C) The c-Myc protein levels in BT-549 cells treated with TM (25 μM).

(D) The levels of c-Myc, SIRT2 and α-tubulin in MCF-7 or BT-549 cells infected with luciferase or SIRT2 shRNAs for 72 hr.

(E) The correlation between the ability of TM to inhibit cancer cell lines and its ability to decrease c-Myc level. The x axis shows the IC_{50} values of TM in different cell lines. The y axis shows the TM-induced decreases in c-Myc level. Relative c-Myc level was obtained by comparing the c-Myc protein level in cells treated with TM for 24 hr with that in vehicle-treated control cells. Error bars represent mean ± SD.

See also Figure S6.

we submitted the TM compound to the Developmental Therapeutics Program of the National Cancer Institute (NCI) at the NIH for screening against the NCI-60 panel of human cancer cell lines (Shoemaker, 2006) at a single dose of 10 μM. The screening result showed that TM inhibited 36 out of 56 of the NCI-60 cell lines by >50% at 10 μM (Figure 7A). In particular, all the leukemia cell lines were very sensitive to TM and most of colon cancer cell lines were sensitive to TM. In contrast, melanoma and ovarian cancer cells were less sensitive to TM. Consistent with our earlier findings (Figure 2), MCF-7 and MDA-MB-468 cells were very sensitive to TM. One discrepancy was noted for MDA-MB-231 cells, which were very sensitive to TM in the NCI-60 screening, but not very sensitive to TM in our study (IC_{50} 34 μM). This could be due to differences in the MDA-MB-231 cells or the culture conditions used in NCI-60 screening and our laboratory. To confirm our findings with MDA-MB-231 cells, we purchased a new batch of MDA-MB-231 cells and showed that the sensitivity to TM was similar to that of the cells we tested earlier (Figure S2D). Despite the discrepancy with MDA-MB-231 cells, the screening results suggest that SIRT2 inhibitors can potentially be used to treat many types of cancers.

To investigate how SIRT2 inhibition halts cancer cell proliferation, we took advantage of NCI molecular target COMPARE analysis (Zaharevitz et al., 2002). NCI has accumulated many datasets regarding the properties of the NCI-60 cell lines, including gene expression, DNA methylation, protein expression, and post-translational modifications. The molecular target COMPARE analysis serves to correlate the response of the NCI-60 panel to a small molecule (TM in this case) to known molecular patterns. From this analysis, we found that the sensitivity of NCI-60 cell lines to TM correlated best with c-Myc phosphorylation/protein levels. In other words, cell lines with higher c-Myc phosphorylation/protein levels were more sensitive to TM (Table S1). The correlation between TM sensitivity and c-Myc is intriguing, as c-Myc is an oncoprotein that is up-regulated in many cancers.

TM Decreases c-Myc Oncoprotein Level in Cancer Cells

The correlation between TM efficacy and c-Myc was informative, but the small correlation value (~0.5) was not sufficient to establish a mechanistic relationship. To further understand the connection, we measured c-Myc level in the cells treated with and without TM or M. TM decreased c-Myc protein level in a time-dependent manner in MCF-7 cells, whereas M treatment had no effect on the c-Myc protein level (Figure 7B). Similar effects of TM on c-Myc were also observed in K562 and MDA-MB-468 cells (Figures S6C and S6D). Consistent with the effect of TM, c-Myc abundance was also reduced by SIRT2 KD (Figure 7D), suggesting that TM works through SIRT2 inhibition to decrease c-Myc. To further establish that the reduction in c-Myc protein is important for the anticancer effect of TM, we examined whether the sensitivity of cancer cell lines to TM correlated with the decrease in c-Myc level induced by TM treatment. Among the six breast cancer cell lines in the NCI-60 panel, BT-549 did not respond to treatment with 10 μM TM. At 10 μM TM, the viability of BT-549 was close to 100%. This result was in line with our own findings (Figure 2B). Although higher concentrations of TM did decrease the viability of BT-549, the sensitivity was much lower than that of MCF-7 cells. Consistent with the reduced sensitivity to TM, SIRT2 KD in BT-549 cells did not decrease cell viability (Figures 3B and S3C). We therefore

examined whether TM could affect c-Myc protein level in BT-549 cells. Consistent with the decreased TM sensitivity, TM treatment did not have a significant effect on c-Myc protein abundance in BT-549 cells (Figure 7C). SIRT2 KD also failed to decrease c-Myc level in BT-549 cells (Figure 7D). These data collectively suggest that the sensitivity of cancer cell lines to TM correlates with the ability of TM to decrease c-Myc level via SIRT2 inhibition in these cell lines. We further measured the IC_{50} values of TM in six different cancer cell lines and the corresponding decrease in c-Myc level in these cell lines upon TM treatment. Plotting the IC_{50} values against the decreases in c-Myc levels indicates that there was an excellent correlation between them (Figure 7E), supporting that the ability of TM to decrease c-Myc is important for its anticancer effect in the cell lines that are very sensitive to TM.

MCF-7 cells were then further analyzed for Myc-specific biological effects. Flow cytometry of TM-treated cells revealed a pronounced increase in cells arrested in G0/G1 phase, with a concomitant decrease of cells in S phase (Figure 8A). Treatment of TM resulted in significant cellular senescence by β-galactosidase staining (Figure 8B). Similar effects of TM on cell cycle progression and cellular senescence were also observed in K562 cells (Figures S6E and S6F), suggesting that the effect of TM-induced c-Myc decrease is not restricted to breast cancer cells. Overall, the phenotypes of G0/G1 cell cycle arrest and cellular senescence are consistent with the anticipated effects of inhibiting cellular c-Myc function (Wu et al., 2007).

To further establish that decreasing c-Myc is important for the anticancer effect of TM, we examined whether forced overexpression of c-Myc in MCF-7 cells is able to reduce TM-mediated cytotoxicity. Cells were transfected with c-Myc for 12 hr before being treated with TM. As shown in Figures 8C and S6G, overexpression of c-Myc significantly reduced the cytotoxicity effect of TM. Together, these results demonstrate TM decreases c-Myc, which is important for the cytotoxicity of TM in tumor cell, although it is likely not the only mechanism that underlies the cytotoxicity.

The *c-Myc* mRNA level was not affected by TM treatment, suggesting that TM does not affect *c-Myc* transcription (Figures 8D and S6H). Therefore, the effect of TM on c-Myc protein turnover was tested. The half-life of c-Myc was shortened by TM treatment, suggesting that TM promoted c-Myc degradation (Figure 8F). Treatment with a proteasome inhibitor, MG132, prevented the TM-induced down-regulation of c-Myc, suggesting that TM promoted the proteasomal degradation of c-Myc (Figure 8E). Increased proteasomal degradation was associated with increased c-Myc ubiquitination (Figure 8G). It was previously reported that SIRT2 can suppress the expression of NEDD4, an E3 ubiquitin ligase for c-Myc (Liu et al., 2013), which could explain why SIRT2 inhibition promotes c-Myc degradation. Indeed, NEDD4 was up-regulated by TM at the transcriptional level (Figures 8H and S6H) and also modestly at the protein level (Figures 8I and S6C) in both MCF-7 and K562 cells. However, this is not a universal mechanism, as alteration of NEDD4 level was not detected in TM-treated MDA-MB-468 cells despite the observed reduction in c-Myc protein abundance (Figures S6D and S6H). As TM regulates the protein stability of c-Myc in all three cell lines, we checked the effect of TM on the transcription levels of several additional known E3 ligases that destabilize c-Myc (Choi et al., 2010; Kim et al., 2003; Liu et al., 2013; Paul et al., 2013; Welcker et al., 2004). As shown in Figure S6H, *NEDD4* and *TRPC4AP* were increased in MCF-7 and K562 cells, but not in MDA-MB-468 cells; *FBXW7* and *STUB1* were up-regulated only in MDA-MB-468 cells; and *FBXO32* was increased in all three cell lines. However, none of the E3 ligase genes was obviously up-regulated by TM in BT-549 cells, in which neither cell viability nor c-Myc level was affected by TM. These results suggested that SIRT2 inhibition led to up-regulation of several c-Myc E3 enzymes, which may result in the destabilization of c-Myc by TM.

DISCUSSION

Previous reports have suggested that SIRT1 or SIRT2 inhibitors can have anticancer activity. However, the potency of most of these inhibitors is modest, with IC_{50} values in the micromolar range at inhibiting purified sirtuins. Most of the sirtuin inhibitors tested for anticancer activity are also not very selective and can inhibit several sirtuins. The modest potency and selectivity make it difficult to rule out off-target effects and pinpoint which sirtuin should be targeted for treating cancers. Our SIRT2 inhibitor TM described here has an excellent combination of potency and selectivity that allowed us to conclude that inhibiting SIRT2 produces anticancer effects in a variety of human cancer cell lines. Knockdown of all seven sirtuins also confirmed that SIRT2 is important for the viability of various cancer cell lines, while knocking down other sirtuins either had no significant effect or much less effect on cancer cell viability.

C-Myc is an important oncoprotein and is up-regulated in many human tumors. Thus, it has been considered as a promising cancer target. So far, no small molecules can directly target c-Myc in vivo. Recent studies showed that bromodomain inhibitors targeting BRD4 can suppress *c-Myc* transcription and inhibit tumorigenesis (Delmore et al., 2011). Our studies demonstrate that inhibiting SIRT2 offers a different way to target c-Myc. We show here that our SIRT2 inhibitor TM can effectively decrease the level of c-Myc in various cancer cell lines. Our data suggest that the ability of TM to decrease c-Myc abundance in different cell lines correlates with the sensitivity of the cell lines to TM. We further demonstrate here that decreasing the c-Myc protein level is an important mechanism that accounts for hypersensitivity of certain cancer cell lines to TM. However, it should be pointed out that effects on other SIRT2-regulated pathways may also contribute to the activity of TM in cancer cells. This is especially true given that even cells without a TM-induced c-Myc decrease (e.g., MDA-MB-231 and BT-549 cells) can still be inhibited by TM at higher concentrations. This also likely explains why c-Myc overexpression confers some but not complete resistance to TM (Figure 8C). We found that TM promotes the proteolytic degradation of c-Myc without affecting its transcription, which serves as an important but perhaps not the only mechanism by which TM destabilizes c-Myc. Aberrant translational control of the Myc oncoprotein has been implicated in many cancers (Chappell et al., 2000; Wolfe et al., 2014) and might also be involved in TM-induced reduction in c-Myc level. Our work establishes SIRT2 inhibition as a strategy to target the oncoprotein c-Myc, which is effective in many human cancer cell lines. Future detailed mechanistic investigations of the

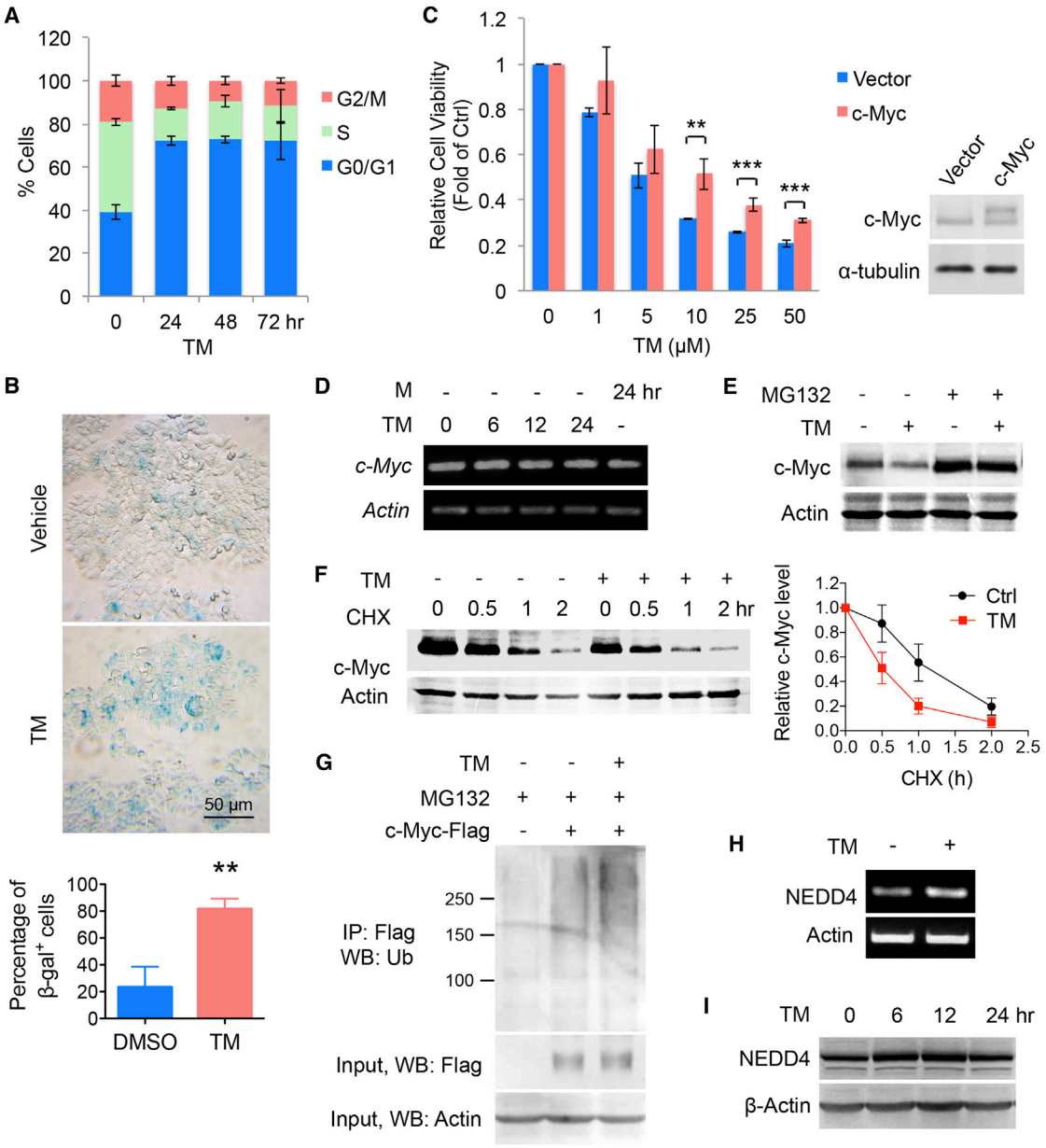

Figure 8. Decreasing c-Myc Protein Abundance Contributes to the Anticancer Effect of TM

(A) Cell cycle distribution (assessed by propidium iodide staining-coupled flow cytometry) of MCF-7 cells treated with TM (25 μM) for 0, 24, 48, or 72 hr.

(B) Acidic β-gal (β-gal) staining in MCF-7 cells treated with TM (25 μM) for 5 days. Representative images are shown in the upper panels and quantification is shown as percentage of β-gal$^+$ cells in the lower panel. Statistical evaluation by two-tailed Student's t test.

(C) Effect of c-Myc overexpression on the cytotoxicity effect of TM. MCF-7 cells were transfected with pCDH vector or pCDH-c-Myc for 12 hr before being treated with TM for 72 hr. Statistical evaluation by two-tailed Student's t test.

(D) The mRNA levels of *c-Myc* in MCF-7 cells treated with TM (25 μM) or M (25 μM) analyzed by RT-PCR.

(E) Effect of MG132 on TM-mediated decrease in c-Myc protein level in MCF-7 cells. Cells were treated with ethanol or TM (25 μM in ethanol) for 4 hr and then MG132 (10 μM) for 2 hr.

(F) Effect of TM on c-Myc degradation in MCF-7 cells. Cells were incubated with ethanol or TM (25 μM in ethanol) for 4 hr and then with CHX (10 μg/ml) for 0, 0.5, 1, or 2 hr. Loading was normalized based on the level of the internal control, actin. The relative c-Myc protein levels at different time point of CHX treatment were calculated by normalizing to the corresponding level without CHX treatment. The relative c-Myc levels were plotted against the time of treatment with CHX.

(G) Effect of TM (25 μM) on the polyubiquitination of c-Myc in MCF-7.

(H) The mRNA level of *NEDD4* in MCF-7 cells treated with TM (25 μM) for 12 hr.

(I) Western blot analysis of NEDD4 protein level in MCF-7 cells treated with TM (25 μM).

Error bars represent mean ± SD. $^{**}p < 0.01$, $^{***}p < 0.001$. See also Figure S6.

SIRT2/c-Myc regulatory pathway could potentially lead to the identification of additional therapeutic targets.

The roles of sirtuins in cancer have been a topic of debate. Both tumor-promoting and tumor-suppressing roles of SIRT1 have been reported. For SIRT2, Kim et al. (2011a) reported that *SIRT2* is a tumor suppressor because *Sirt2* KO mice develop tumors earlier than WT mice. Serrano et al. (2013) did not find a cancer-prone phenotype in unchallenged *Sirt2* KO mice that they generated, although they did observe that *Sirt2* KO mice had increased tumorigenesis when challenged with carcinogens. Contrary to these genetic studies that pointed to a weak tumor-suppressor role of SIRT2, we found that inhibiting SIRT2 with TM has broad anticancer activity in many cancer cell lines.

Different outcomes for mouse genetic studies and pharmacological studies in cancer cells are not without precedent. Similar cases have been well documented in the literature (Weiss et al., 2007). There are several possible explanations. First, there are several examples of factors that have tumor-suppressor activity in normal cells but nevertheless are required for the growth and survival of transformed cells. For example, loss of function for the DNA-damage checkpoint kinase ATR causes modest tumor predisposition but greatly impairs the growth of established tumors (Bartek et al., 2012). SIRT2 has been identified as a regulator of mitotic chromosome segregation (Kim et al., 2011a), a function that could account for the weak tumor predisposition phenotype in *Sirt2*-deficient mice given the oncogenic consequences of genomic instability. Nevertheless, a greater dependency of transformed cells on SIRT2 due to increased mitotic and other stresses, or because of the regulation of other targets such as c-Myc by SIRT2, results in heightened sensitivity to SIRT2 inhibition in cancer cells. It also should be noted that small molecules may have off-target effects, which could contribute to observed pharmacological effects. While it is difficult to completely rule out this possibility for the anticancer effect of TM, our studies using the inactive control compound (M) and the SIRT2 KD studies suggest that the anticancer effect is largely through SIRT2 inhibition.

An alternative explanation relates to the fact that in a genetic KO, the protein is gone and thus all the enzymatic activities and protein-protein interactions involving the enzyme also are gone. In contrast, when using a small molecule to inhibit the enzyme, the protein is intact and so are the protein-protein interactions that involve the protein. In the case of SIRT2, another layer of complexity is that SIRT2 has multiple enzymatic functions. We and others recently found that sirtuins are not only deacetylases. Some sirtuins, such as SIRT5 (Du et al., 2011) and SIRT6 (Jiang et al., 2013), prefer to hydrolyze other acyl lysine modifications. Perhaps more surprising is the fact that even the well-studied deacetylases (SIRT1, SIRT2, and SIRT3) can remove long-chain fatty acyl groups efficiently (He et al., 2014; Liu et al., 2014). Although the exact substrate proteins for the defatty-acylase activity of SIRT2 remain to be identified, our preliminary studies showed that the fatty-acylation levels of many proteins were elevated when SIRT2 was knocked down (Figure S4B), but not when the SIRT2 inhibitor TM was used (Figure S4C). Thus, the small-molecule inhibitor may selectively target one of the enzymatic functions of SIRT2, thus contributing to the fact that small-molecule inhibitors may produce beneficial pharmacological effects that are different from genetic KO.

EXPERIMENTAL PROCEDURES

For more details, see Supplemental Experimental Procedures.

Synthesis of Compounds

Detailed synthetic routes are presented in Supplemental Experimental Procedures. The nuclear magnetic resonance spectra of the synthesized compounds are shown in Figure S7.

Inhibition Assay for Different Sirtuins

The assays were carried out using a high-performance liquid chromatography-based method with different acyl peptides. The detailed method is described in Supplemental Experimental Procedures.

Cell Viability Assay

Cells were seeded into 96-well plates at 3,000–4,000 cells per well. After 24 hr, test compounds were added to cells to final concentrations ranging from 1 to 50 μM. Cells were then incubated for 72 hr and cell viability was measured using the CellTiter-Blue viability assay (Promega) following the manufacturer's instructions. Relative cell viability in the presence of test compounds was normalized to the vehicle-treated controls after background subtraction. GraphPad Prism software was used to determine the IC_{50} values.

Knockdown of SIRT1-7 in various cell lines was achieved by lentiviral infection. Lentiviral supernatants were generated as described previously (Jiang et al., 2013). Cell viability was assessed after 3, 5, or 10 days of infection by using CellTiter-Blue.

Animal Experiments

All animals used in this study were handled in accordance with federal and institutional guidelines, under a protocol approved by the Cornell University Institutional Animal Care and Use Committee. For more animal experimental details, see Supplemental Experimental Procedures.

Statistical Analysis

Quantitative data were expressed as mean ± SD (shown as error bar) from at least three independent experiments. Differences between two groups were examined statistically as indicated (*$p < 0.05$, **$p < 0.01$, and ***$p < 0.001$).

SUPPLEMENTAL INFORMATION

Supplemental Information includes Supplemental Experimental Procedures, seven figures, and one table and can be found with this article online at http://dx.doi.org/10.1016/j.ccell.2016.02.007.

AUTHOR CONTRIBUTIONS

H.J. designed and performed all the biochemical studies except those noted below. B.H. and H.L. designed the sirtuin inhibitors. J.H., B.H., and Y.L.C. synthesized the inhibitors and biotin-conjugated compounds. H.J., J.H., and B.H. purified the sirtuin enzymes, performed in vitro inhibitor assay, and determined the mechanism of SIRT2 inhibition. Y.L.N.A. and J.S. performed the animal studies. K.W., M.C., and P.G. carried out the Biotin-TM pull-down assay and immunofluorescence of acetyl-α-tubulin. P.G. suggested the NCI60 screening, which helped in making the c-Myc connection. T.S. performed pathologic review. R.S.W. directed the animal studies. H.L. directed the inhibitor development and biochemical studies, and wrote the manuscript with help from H.J., R.S.W., P.G., J.H., and Y.L.N.A.

ACKNOWLEDGMENTS

We thank the Development Therapeutic Program at the National Cancer Institute for screening TM in the NCI60 cell lines. This work is supported in part by an intercampus seed grant from Cornell University and a transformative R01

grant from NIH (CA163255). YLNA is supported by NIH/NIGMS grant 5T32GM008500.

Received: February 13, 2015
Revised: July 3, 2015
Accepted: February 8, 2016
Published: March 14, 2016

REFERENCES

Bartek, J., Mistrik, M., and Bartkova, J. (2012). Thresholds of replication stress signaling in cancer development and treatment. Nat. Struct. Mol. Biol. *19*, 5–7.

Beroukhim, R., Mermel, C.H., Porter, D., Wei, G., Raychaudhuri, S., Donovan, J., Barretina, J., Boehm, J.S., Dobson, J., Urashima, M., et al. (2010). The landscape of somatic copy-number alteration across human cancers. Nature *463*, 899–905.

Chappell, S.A., LeQuesne, J.P., Paulin, F.E., deSchoolmeester, M.L., Stoneley, M., Soutar, R.L., Ralston, S.H., Helfrich, M.H., and Willis, A.E. (2000). A mutation in the c-myc-IRES leads to enhanced internal ribosome entry in multiple myeloma: a novel mechanism of oncogene de-regulation. Oncogene *19*, 4437–4440.

Chen, J., Chan, A.W., To, K.F., Chen, W., Zhang, Z., Ren, J., Song, C., Cheung, Y.S., Lai, P.B., Cheng, S.H., et al. (2013). SIRT2 overexpression in hepatocellular carcinoma mediates epithelial to mesenchymal transition by protein kinase B/glycogen synthase kinase-3beta/beta-catenin signaling. Hepatology *57*, 2287–2298.

Cheon, M.G., Kim, W., Choi, M., and Kim, J.E. (2015). AK-1, a specific SIRT2 inhibitor, induces cell cycle arrest by downregulating Snail in HCT116 human colon carcinoma cells. Cancer Lett. *356*, 637–645.

Choi, S.H., Wright, J.B., Gerber, S.A., and Cole, M.D. (2010). Myc protein is stabilized by suppression of a novel E3 ligase complex in cancer cells. Genes Dev. *24*, 1236–1241.

Delmore, J.E., Issa, G.C., Lemieux, M.E., Rahl, P.B., Shi, J., Jacobs, H.M., Kastritis, E., Gilpatrick, T., Paranal, R.M., Qi, J., et al. (2011). BET bromodomain inhibition as a therapeutic strategy to target c-Myc. Cell *146*, 904–917.

Di Fruscia, P., Ho, K.K., Laohasinnarong, S., Khongkow, M., Kroll, S.H., Islam, S.A., Sternberg, M.J., Schmidtkunz, K., Jung, M., Lam, E.W., and Fuchter, M.J. (2012). The discovery of novel 10,11-dihydro-5H-dibenz[b,f]azepine SIRT2 inhibitors. Medchemcomm. http://dx.doi.org/10.1039/C2MD00290F.

Du, J., Zhou, Y., Su, X., Yu, J., Khan, S.H., Kim, J., Woo, J., Kim, J.H., Choi, B.H., et al. (2011). Sirt5 is an NAD-dependent protein lysine demalonylase and desuccinylase. Science *334*, 806–809.

Fang, Y., and Nicholl, M.B. (2011). Sirtuin 1 in malignant transformation: friend or foe? Cancer Lett. *306*, 10–14.

Fatkins, D.G., Monnot, A.D., and Zheng, W. (2006). Nε-Thioacetyl-lysine: a multi-facet functional probe for enzymatic protein lysine Nε-deacetylation. Bioorg. Med. Chem. Lett. *16*, 3651–3656.

Feldman, J.L., Baeza, J., and Denu, J.M. (2013). Activation of the protein deacetylase SIRT6 by long-chain fatty acids and widespread deacylation by mammalian sirtuins. J. Biol. Chem. *288*, 31350–31356.

Guy, C.T., Cardiff, R.D., and Muller, W.J. (1992). Induction of mammary tumors by expression of polyomavirus middle T oncogene: a transgenic mouse model for metastatic disease. Mol. Cell Biol. *12*, 954–961.

Haigis, M.C., and Sinclair, D.A. (2010). Mammalian sirtuins: biological insights and disease relevance. Annu. Rev. Pathol. *5*, 253–295.

Hawse, W.F., Hoff, K.G., Fatkins, D.G., Daines, A., Zubkova, O.V., Schramm, V.L., Zheng, W., and Wolberger, C. (2008). Structural insights into intermediate steps in the Sir2 deacetylation reaction. Structure *16*, 1368–1377.

He, B., Du, J., and Lin, H. (2012). Thiosuccinyl peptides as Sirt5-specific inhibitors. J. Am. Chem. Soc. *134*, 1922–1925.

He, B., Hu, J., Zhang, X., and Lin, H. (2014). Thiomyristoyl peptides as cell-permeable Sirt6 inhibitors. Org. Biomol. Chem. *12*, 7498–7502.

Heltweg, B., Gatbonton, T., Schuler, A.D., Posakony, J., Li, H., Goehle, S., Kollipara, R., Depinho, R.A., Gu, Y., Simon, J.A., and Bedalov, A. (2006). Antitumor activity of a small-molecule inhibitor of human silent information regulator 2 enzymes. Cancer Res. *66*, 4368–4377.

Herranz, D., and Serrano, M. (2010). SIRT1: recent lessons from mouse models. Nat. Rev. Cancer *10*, 819–823.

Hoffmann, G., Breitenbucher, F., Schuler, M., and Ehrenhofer-Murray, A.E. (2014). A novel sirtuin 2 (SIRT2) inhibitor with p53-dependent pro-apoptotic activity in non-small cell lung cancer. J. Biol. Chem. *289*, 5208–5216.

Imai, S.-i., and Guarente, L. (2010). Ten years of NAD-dependent SIR2 family deacetylases: implications for metabolic diseases. Trends Pharmacol. Sci. *31*, 212–220.

Imai, S.-i., Armstrong, C.M., Kaeberlein, M., and Guarente, L. (2000). Transcriptional silencing and longevity protein Sir2 is an NAD-dependent histone deacetylase. Nature *403*, 795–800.

Jiang, H., Khan, S., Wang, Y., Charron, G., He, B., Sebastian, C., Du, J., Kim, R., Ge, E., Mostoslavsky, R., et al. (2013). SIRT6 regulates TNF-alpha secretion through hydrolysis of long-chain fatty acyl lysine. Nature *496*, 110–113.

Kim, S.Y., Herbst, A., Tworkowski, K.A., Salghetti, S.E., and Tansey, W.P. (2003). Skp2 regulates Myc protein stability and activity. Mol. Cell *11*, 1177–1188.

Kim, H.S., Vassilopoulos, A., Wang, R.H., Lahusen, T., Xiao, Z., Xu, X., Li, C., Veenstra, T.D., Li, B., Yu, H., et al. (2011a). SIRT2 maintains genome integrity and suppresses tumorigenesis through regulating APC/C activity. Cancer Cell *20*, 487–499.

Kim, W.J., Lee, J.W., Quan, C., Youn, H.J., Kim, H.M., and Bae, S.C. (2011b). Nicotinamide inhibits growth of carcinogen induced mouse bladder tumor and human bladder tumor xenograft through up-regulation of RUNX3 and p300. J. Urol. *185*, 2366–2375.

Lee, J.-H., Choy, M.L., and Marks, P.A. (2012). Mechanisms of resistance to histone deacetylase inhibitors. Adv. Cancer Res. *116*, 39–86.

Liu, P.Y., Xu, N., Malyukova, A., Scarlett, C.J., Sun, Y.T., Zhang, X.D., Ling, D., Su, S.P., Nelson, C., Chang, D.K., et al. (2013). The histone deacetylase SIRT2 stabilizes Myc oncoproteins. Cell Death Differ. *20*, 503–514.

Liu, Z., Yang, T., Li, X., Peng, T., Hang, H.C., and Li, X.D. (2014). Integrative chemical biology approaches for identification and characterization of "erasers" for fatty-acid-acylated lysine residues within proteins. Angew. Chem. Int. Ed. Engl. *54*, 1149–1152.

Mahajan, S.S., Scian, M., Sripathy, S., Posakony, J., Lao, U., Loe, T.K., Leko, V., Thalhofer, A., Schuler, A.D., Bedalov, A., and Simon, J.A. (2014). Development of pyrazolone and isoxazol-5-one cambinol analogues as sirtuin inhibitors. J. Med. Chem. *57*, 3283–3294.

Marks, P.A., and Breslow, R. (2007). Dimethyl sulfoxide to vorinostat: development of this histone deacetylase inhibitor as an anticancer drug. Nat. Biotechnol. *25*, 84–90.

McCarthy, A.R., Sachweh, M.C., Higgins, M., Campbell, J., Drummond, C.J., van Leeuwen, I.M., Pirrie, L., Ladds, M.J., Westwood, N.J., and Lain, S. (2013). Tenovin-D3, a novel small-molecule inhibitor of sirtuin SirT2, increases p21 (CDKN1A) expression in a p53-independent manner. Mol. Cancer Ther. *12*, 352–360.

McGlynn, L.M., Zino, S., MacDonald, A.I., Curle, J., Reilly, J.E., Mohammed, Z.M., McMillan, D.C., Mallon, E., Payne, A.P., Edwards, J., and Shiels, P.G. (2014). SIRT2: tumour suppressor or tumour promoter in operable breast cancer? Eur. J. Cancer *50*, 290–301.

Meyer, N., and Penn, L.Z. (2008). Reflecting on 25 years with MYC. Nat. Rev. Cancer *8*, 976–990.

Neugebauer, R.C., Uchiechowska, U., Meier, R., Hruby, H., Valkov, V., Verdin, E., Sippl, W., and Jung, M. (2008). Structure-activity studies on splitomicin derivatives as sirtuin inhibitors and computational prediction of binding mode. J. Med. Chem. *51*, 1203–1213.

Paul, I., Ahmed, S.F., Bhowmik, A., Deb, S., and Ghosh, M.K. (2013). The ubiquitin ligase CHIP regulates c-Myc stability and transcriptional activity. Oncogene *32*, 1284–1295.

Peng, C., Lu, Z., Xie, Z., Cheng, Z., Chen, Y., Tan, M., Luo, H., Zhang, Y., He, W., Yang, K., et al. (2011). The first identification of lysine malonylation substrates and its regulatory enzyme. Mol. Cell. Proteomics *10*, M111.012658.

Rotili, D., Tarantino, D., Nebbioso, A., Paolini, C., Huidobro, C., Lara, E., Mellini, P., Lenoci, A., Pezzi, R., Botta, G., et al. (2012). Discovery of salermide-related sirtuin inhibitors: binding mode studies and antiproliferative effects in cancer cells including cancer stem cells. J. Med. Chem. *55*, 10937–10947.

Seifert, T., Malo, M., Kokkola, T., Engen, K., Friden-Saxin, M., Wallen, E.A., Lahtela-Kakkonen, M., Jarho, E.M., and Luthman, K. (2014). Chroman-4-one- and chromone-based sirtuin 2 inhibitors with antiproliferative properties in cancer cells. J. Med. Chem. *57*, 9870–9888.

Serrano, L., Martinez-Redondo, P., Marazuela-Duque, A., Vazquez, B.N., Dooley, S.J., Voigt, P., Beck, D.B., Kane-Goldsmith, N., Tong, Q., Rabanal, R.M., et al. (2013). The tumor suppressor SirT2 regulates cell cycle progression and genome stability by modulating the mitotic deposition of H4K20 methylation. Genes Dev. *27*, 639–653.

Shoemaker, R.H. (2006). The NCI60 human tumour cell line anticancer drug screen. Nat. Rev. Cancer *6*, 813–823.

Smith, B.C., and Denu, J.M. (2007). Mechanism-based Inhibition of Sir2 deacetylases by thioacetyl-lysine peptide. Biochemistry *46*, 14478–14486.

Soung, Y.H., Pruitt, K., and Chung, J. (2014). Epigenetic silencing of ARRDC3 expression in basal-like breast cancer cells. Sci. Rep. *4*, 3846.

Stünkel, W., and Campbell, R.M. (2011). Sirtuin 1 (SIRT1): the misunderstood HDAC. J. Biomol. Screen. *16*, 1153–1169.

Suzuki, T., Asaba, T., Imai, E., Tsumoto, H., Nakagawa, H., and Miyata, N. (2009). Identification of a cell-active non-peptide sirtuin inhibitor containing N-thioacetyl lysine. Bioorg. Med. Chem. Lett. *19*, 5670–5672.

Teng, Y.B., Jing, H., Aramsangtienchai, P., He, B., Khan, S., Hu, J., Lin, H., and Hao, Q. (2015). Efficient demyristoylase activity of SIRT2 revealed by kinetic and structural studies. Sci. Rep. *5*, 8529.

Weiss, W.A., Taylor, S.S., and Shokat, K.M. (2007). Recognizing and exploiting differences between RNAi and small-molecule inhibitors. Nat. Chem. Biol. *3*, 739–744.

Welcker, M., Orian, A., Jin, J., Grim, J.E., Harper, J.W., Eisenman, R.N., and Clurman, B.E. (2004). The Fbw7 tumor suppressor regulates glycogen synthase kinase 3 phosphorylation-dependent c-Myc protein degradation. Proc. Natl. Acad. Sci. USA *101*, 9085–9090.

Wolfe, A.L., Singh, K., Zhong, Y., Drewe, P., Rajasekhar, V.K., Sanghvi, V.R., Mavrakis, K.J.M., Roderick, J.E., Van der Meulen, J., Schatz, J.H., et al. (2014). RNA G-quadruplexes cause eIF4A-dependent oncogene translation in cancer. Nature *513*, 65–70.

Wu, C.H., van Riggelen, J., Yetil, A., Fan, A.C., Bachireddy, P., and Felsher, D.W. (2007). Cellular senescence is an important mechanism of tumor regression upon c-Myc inactivation. Proc. Natl. Acad. Sci. USA *104*, 13028–13033.

Yang, M.H., Laurent, G., Bause, A.S., Spang, R., German, N., Haigis, M.C., and Haigis, K.M. (2013). HDAC6 and SIRT2 regulate the acetylation state and oncogenic activity of mutant K-RAS. Mol. Cancer Res. *11*, 1072–1077.

Yoon, Y.K., Ali, M.A., Wei, A.C., Shirazi, A.N., Parang, K., and Choon, T.S. (2014). Benzimidazoles as new scaffold of sirtuin inhibitors: green synthesis, in vitro studies, molecular docking analysis and evaluation of their anti-cancer properties. Eur. J. Med. Chem. *83*, 448–454.

Zaharevitz, D.W., Holbeck, S.L., Bowerman, C., and Svetlik, P.A. (2002). COMPARE: a web accessible tool for investigating mechanisms of cell growth inhibition. J. Mol. Graph Model. *20*, 297–303.

Zhang, Y., Au, Q., Zhang, M., Barber, J.R., Ng, S.C., and Zhang, B. (2009). Identification of a small molecule SIRT2 inhibitor with selective tumor cytotoxicity. Biochem. Biophys. Res. Commun. *386*, 729–733.

Zhao, D., Zou, S.-W., Liu, Y., Zhou, X., Mo, Y., Wang, P., Xu, Y.-H., Dong, B., Xiong, Y., Lei, Q.-Y., and Guan, K.-L. (2013). Lysine-5 acetylation negatively regulates lactate dehydrogenase A and is decreased in pancreatic cancer. Cancer Cell *23*, 464–476.

Zhao, D., Mo, Y., Li, M.T., Zou, S.W., Cheng, Z.L., Sun, Y.P., Xiong, Y., Guan, K.L., and Lei, Q.Y. (2014). NOTCH-induced aldehyde dehydrogenase 1A1 deacetylation promotes breast cancer stem cells. J. Clin. Invest. *124*, 5453–5465.

Zhu, A.Y., Zhou, Y., Khan, S., Deitsch, K.W., Hao, Q., and Lin, H. (2012). *Plasmodium falciparum* Sir2A preferentially hydrolyzes medium and long chain fatty acyl lysine. ACS Chem. Biol. *7*, 155–159.

Cancer Cell, Volume *29*

Supplemental Information

A SIRT2-Selective Inhibitor Promotes c-Myc Oncoprotein Degradation and Exhibits Broad Anticancer Activity

Hui Jing, Jing Hu, Bin He, Yashira L. Negrón Abril, Jack Stupinski, Keren Weiser, Marisa Carbonaro, Ying-Ling Chiang, Teresa Southard, Paraskevi Giannakakou, Robert S. Weiss, and Hening Lin

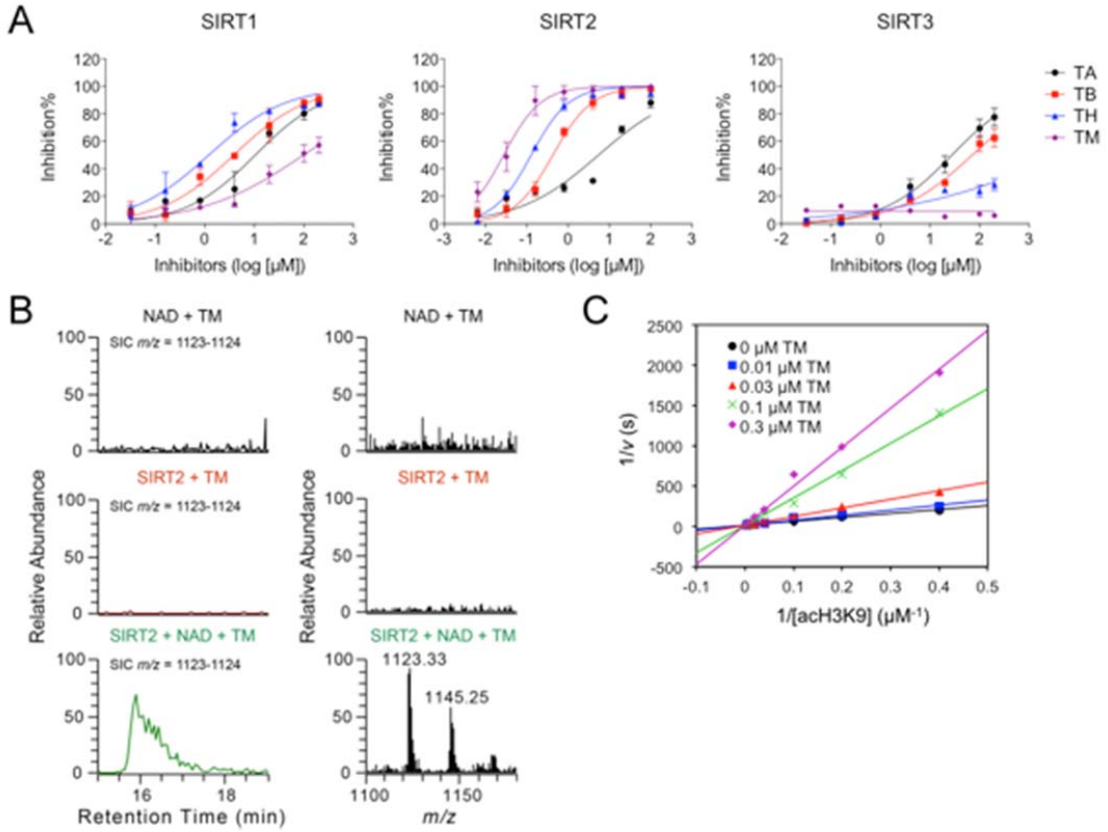

Figure S1. Related to Figure 1. (**A**) Dose-responsive curve for TA, TB, TH, TM and M against SIRT1-3. (**B**) LC-MS detection of the covalent intermediate formed by TM and NAD. The selected ion chromatogram (SIC) (*m/z* = 1123-1124) was shown on the left, the mass spectrum was shown on the right. The data from the reaction mixture containing 100 μM NAD, 100 μM TM, 1 mM DTT, and 20 mM pyridinium formate (pH 7.0) or the mixture containing 50 μM SIRT2, 100 μM TM, 1 mM DTT, and 20 mM Pyridinium formate (pH 7.0) were shown as negative controls. (**C**) Double reciprocal plot with varied TM and acH3K9 concentrations. Data was fit to competitive inhibition using Graphpad Prism. Error bars represent mean ± sd.

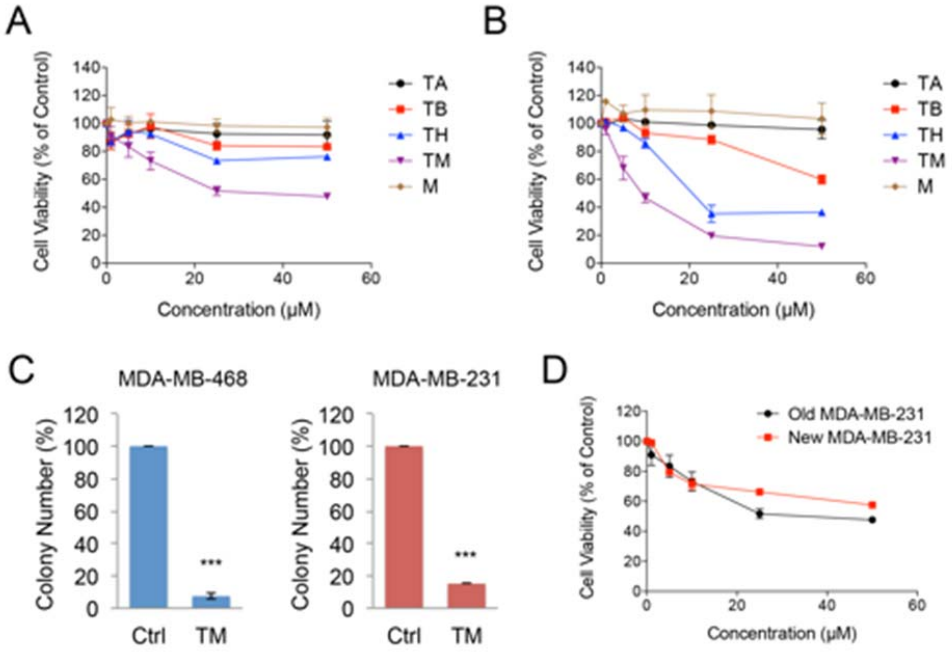

Figure S2. Related to Figure 2. (**A and B**) Cell viability of MDA-MB-231 (**A**) and HeLa (**B**) cells treated with ethanol or indicated inhibitors (1, 5, 10, 25, 50 μM) for 72 hr. (**C**) Soft agar colony formation of MDA-MB-468 and MDA-MB-231 cells treated with ethanol or TM (25 μM). The y axis represents percent colony number relative to ethanol-treated cells. Statistics, two-tailed Student's *t*-test. (**D**) Comparison of the sensitivity of two batches of MDA-MB-231 cells to TM treatment. The old MDA-MB-231 cell line has been maintained in our laboratory for over 2 years; while the new MDA-MB-231 cell line has been recently purchased from ATCC. Cells were seeded in 96-well plate one day before TM treatment at a density of 3,000/well. On the day of treatment, cells were incubated with media containing 0, 1, 5, 10, 25, and 50 μM for TM for 3 days. CellTiter-Blue® assay was performed to assess the cell viability. Error bars represent mean ± sd. ***$p < 0.001$.

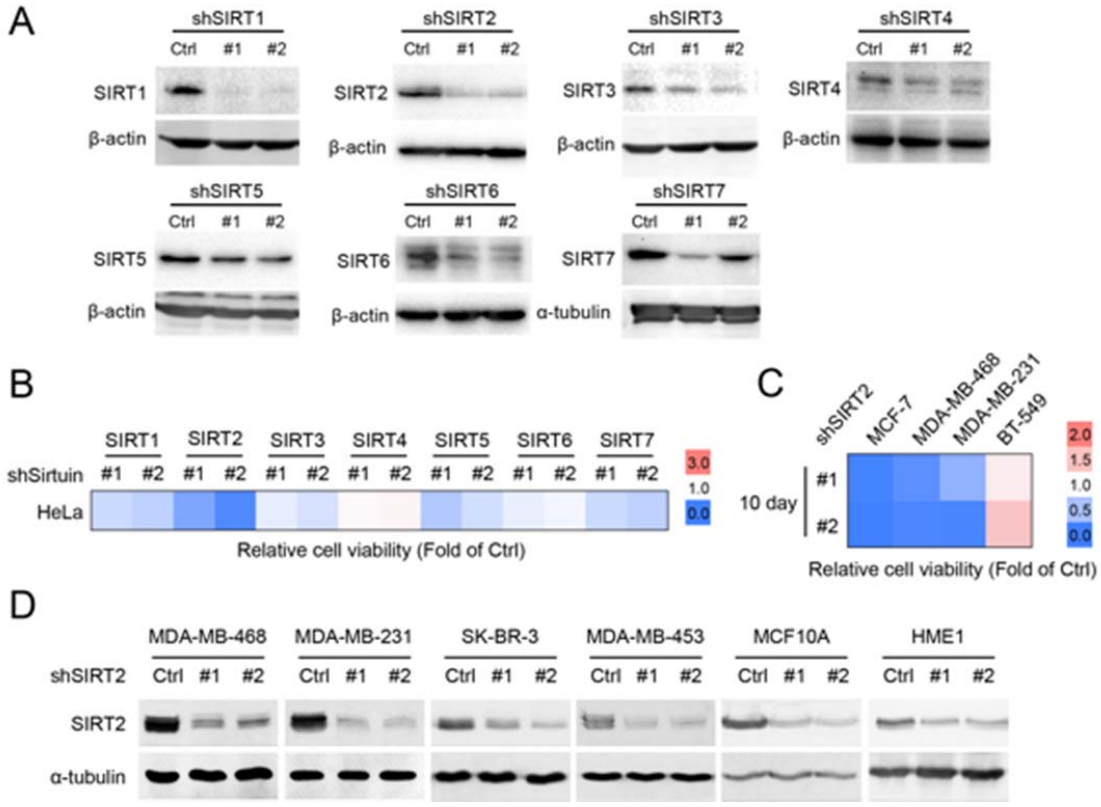

Figure S3. Related to Figure 3. (**A**) Representative results showing the knockdown efficiency of SIRT1-7 in HeLa cells. Cells were infected with lentivirus carrying Luciferase shRNA and shRNAs against SIRT1-7 for 72 hr before analyzed by Western blot for sirtuin levels. (**B**) Cytotoxicity effects of knocking down SIRT1-7 in HeLa cells after 72 hr of lentiviral infection. (**C**) Cytotoxicity effects of SIRT2 knockdown in MCF-7, MDA-MB-468, MDA-MB-231 and BT-549 cells at day 10 after the infection. (**D**) SIRT2 knockdown efficiency in Figure 3B and Figure S3C was confirmed by Western blot (the first row). The α-tubulin level was used as internal standard of total protein amount.

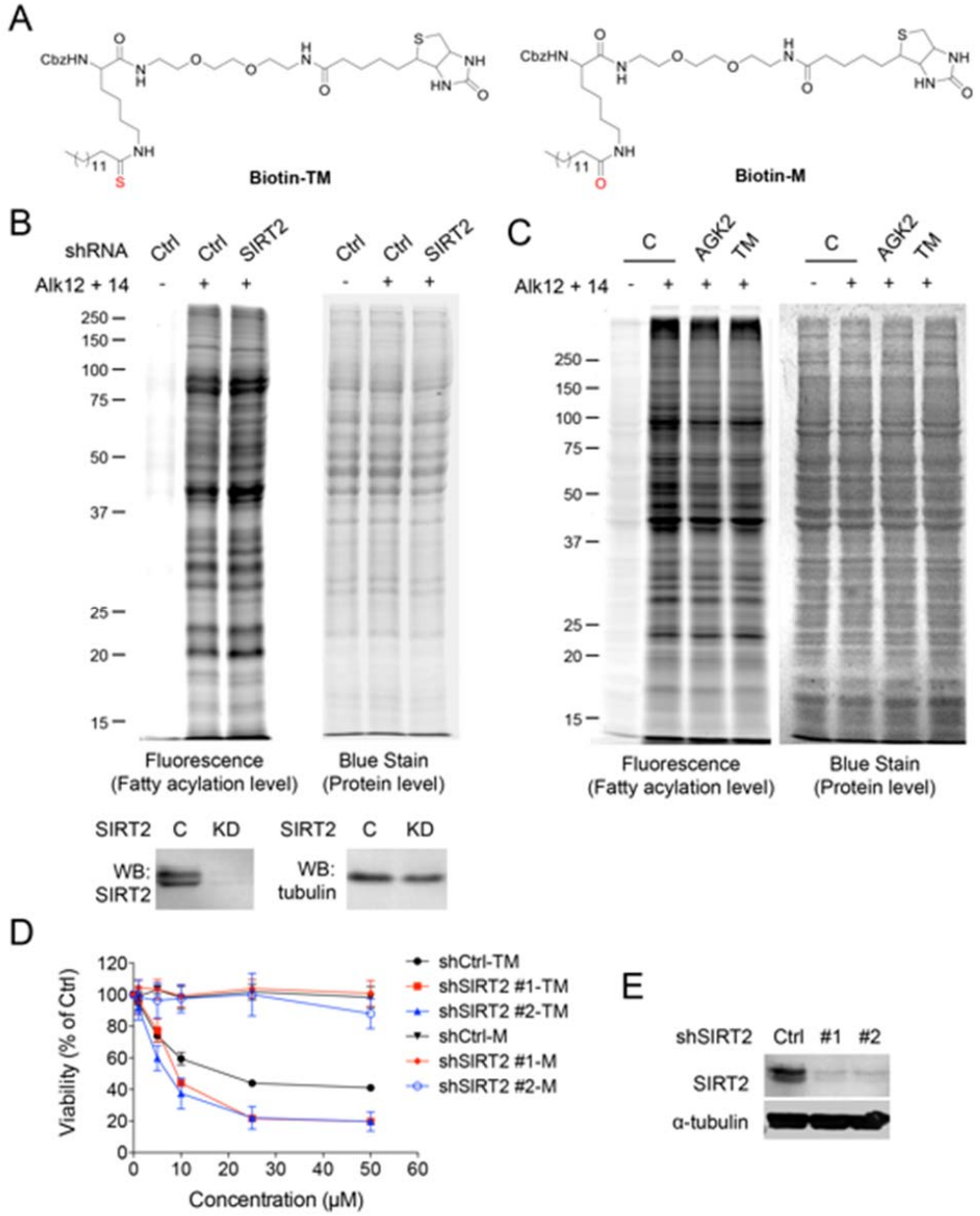

Figure S4.

Related to Figure 4. (**A**) Structures of Biotin-TM and Biotin-M. (**B**) Global protein fatty-acylation in HEK293T cells with Ctrl and SIRT2 knockdown. Protein fatty acylation was detected by a metabolic labeling method using alkyne-tagged fatty acid analogs Alk12 (50 μM) and Alk14 (50 μM) as previously reported (Jiang et al., 2013). (**C**) Global protein fatty acylation in HEK293T cells treated with the ethanol, AGK2 (25 μM) or TM (25 μM) for 6 hr in the presence of Alk12 (50 μM) and Alk14 (50 μM). (**D**) Effect of SIRT2 knockdown on the sensitivity of MDA-MB-231 cells to TM. MDA-MB-231 cells were infected with lentiviral Luciferase shRNA and SIRT2 shRNAs, respectively, for 24 hr before being treated with different concentrations of TM for another 72 hr. Cell viability was measured by CellTiter-Blue® assay. (**E**) SIRT2 knockdown in (**D**) was confirmed after 72 hr of infection by Western blot. Error bars represent mean ± sd.

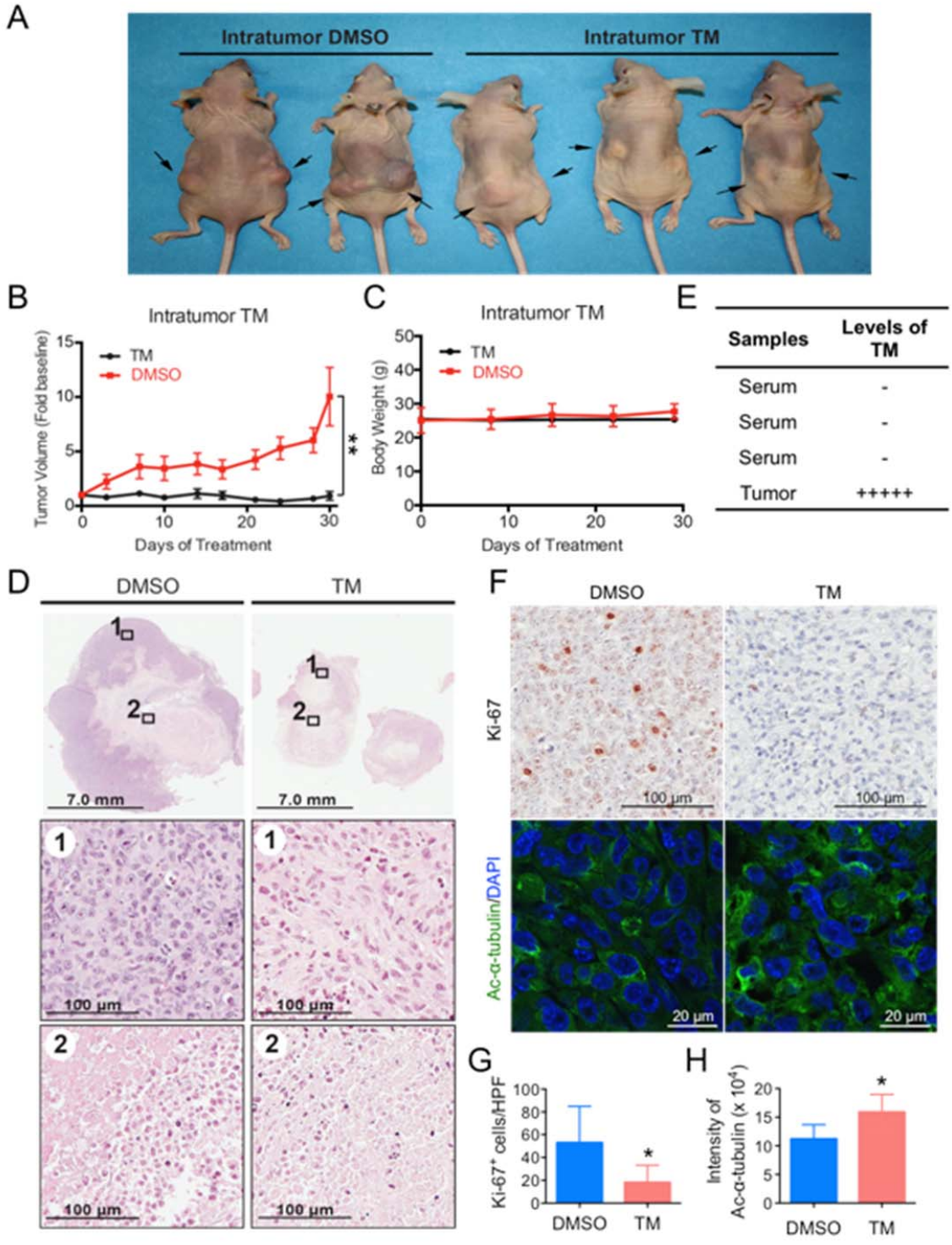

Figure S5. Related to Figure 5. Analysis of tumor growth and histopathological findings of xenografted mice treated by intratumor TM injection. Mice bearing MDA-MB-231 human breast cancer xenograft were divided into two groups and treated by direct intratumor injection with either

the control vehicle solvent (DMSO) or TM (0.75 mg TM in 50 uL DMSO; n = 5) three times per week. Tumors were collected after 30-day treatment. (**A**) Gross findings at necropsy after 30 days of intratumor treatment with either DMSO or TM. (**B**) Tumor growth chart. Statistics, paired Student's *t*-test. (**C**) Mouse body weight chart. (**D**) Hematoxylin and eosin staining of tumor tissues after 30 days of treatment with either DMSO or TM. (**E**) Detection of TM in mouse serum and tumor tissues by mass spectrometry. (**F**) Representative images of Ki-67 immunohistochemistry staining and acetyl-α-tubulin (K40) immunofluorescence staining of tumor tissues after 30 days of treatment with either DMSO or TM. (**G**) Quantification of Ki-67^+ cells in (**F**). The y axis represents Ki-67^+ cells per high power field (10 HPFs/tumor for all the tumors analyzed, n = 4 for DMSO, n = 6 for TM). Statistics, unpaired Student's *t*-test. (**H**) Quantification of acetyl-α-tubulin fluorescence intensity in (**F**). The y axis represents integrated intensity per cell. (10 HPFs/tumor for all the tumors analyzed, n = 4 for DMSO, n = 6 for TM). Statistics, unpaired Student's *t*-test. Error bars represent mean ± sd. *$p < 0.05$, **$p < 0.01$.

Table S1. Related to Figure 7. Top four correlated genes from molecular target Compare analysis of the NCI-60 assay data of TM. The data set used is the MT series.

Rank	**Mol. Target ID**	**Gene**	**Correlation value**	**Target pattern description**
1	MT18283	*MYC*	0.503	c-Myc phosphorylation level at T58 and S62
2	MT18332	*MYC*	0.493	c-Myc protein level
3	MT11065	*FGFR2*	0.477	Fraction of DNA methylation at *FGFR2* 5' UTR
4	MT1125	*CDC25A*	0.465	Relative mRNA levels of *CDC25A*

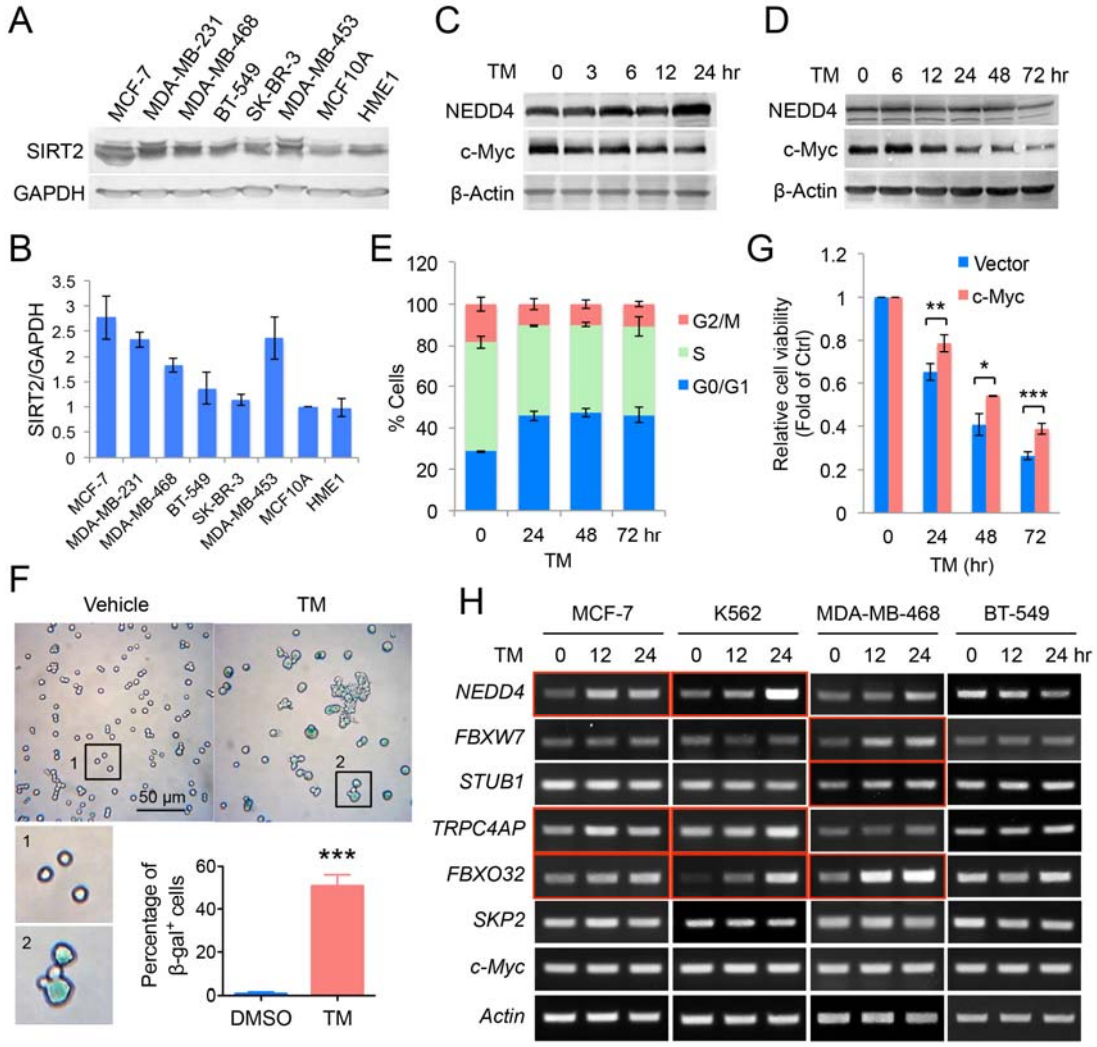

Figure S6. Relate to Figure 8. (**A, B**) SIRT2 levels in different human normal and breast cancer cell lines. Western blot analysis of SIRT2 level (**A**) and semi-quantification of SIRT2 level relative to GAPDH level (**B**). (**C, D**) Effects of TM on c-Myc and NEDD4 protein levels in K562 (**C**) and MDA-MB-468 (**D**) cells. Cells were treated as indicated. (**E**) Cell cycle distribution of K562 cells treated with TM (25 μM) for 0, 24, 48 or 72 hr. The graph shows the percentage of cells for each cell cycle phase as assessed by propidium iodide (PI) staining-coupled flow cytometry. (**F**) Acidic β-gal (β-gal) staining in K562 cells treated with TM (25 μM) for 5 days. Quantification (right panel) was shown as percentage of β-gal^{+} cells. Statistics, two-tailed Student's *t*-test. (**G**) Effect of c-Myc overexpression on the cytotoxicity effect of TM. MCF-7 cells transfected with pCDH vector or pCHD-c-*Myc* for 12 hr were treated with TM (25 μM) for another 0, 24, 48 or 72 hr, followed by CellTiter-Blue® assay. (**H**) Effect of TM on the transcript levels of various E3 ligases of c-Myc. MCF-7, K562, MDA-MB-468 or BT-549 cells were treated with TM (25 μM) for the indicated time. PCR was performed for the assessment of transcript levels of E3 ligases (*NEDD4, FBXW7, STUB1, TRPC4AP, FBXO32, SKP2*), *c-Myc* and *Actin*. Statistics, two-tailed Student's *t*-test. Error bars represent mean ± sd. *p < 0.05, **p < 0.01, ***p < 0.001.

A

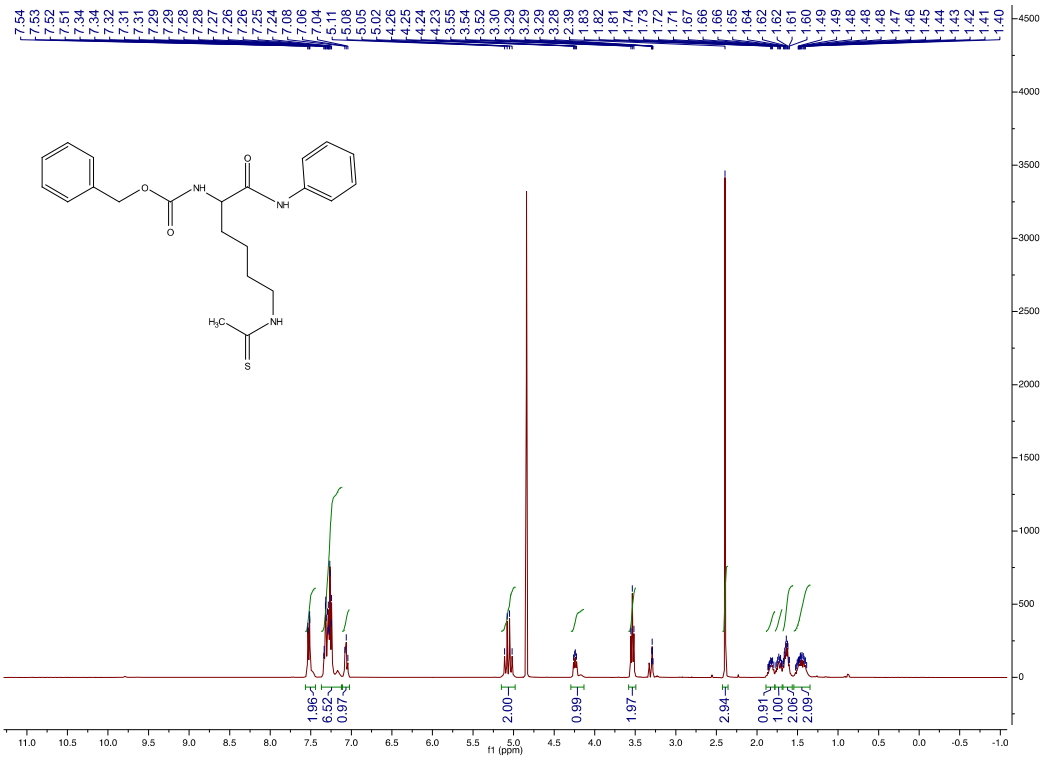

B

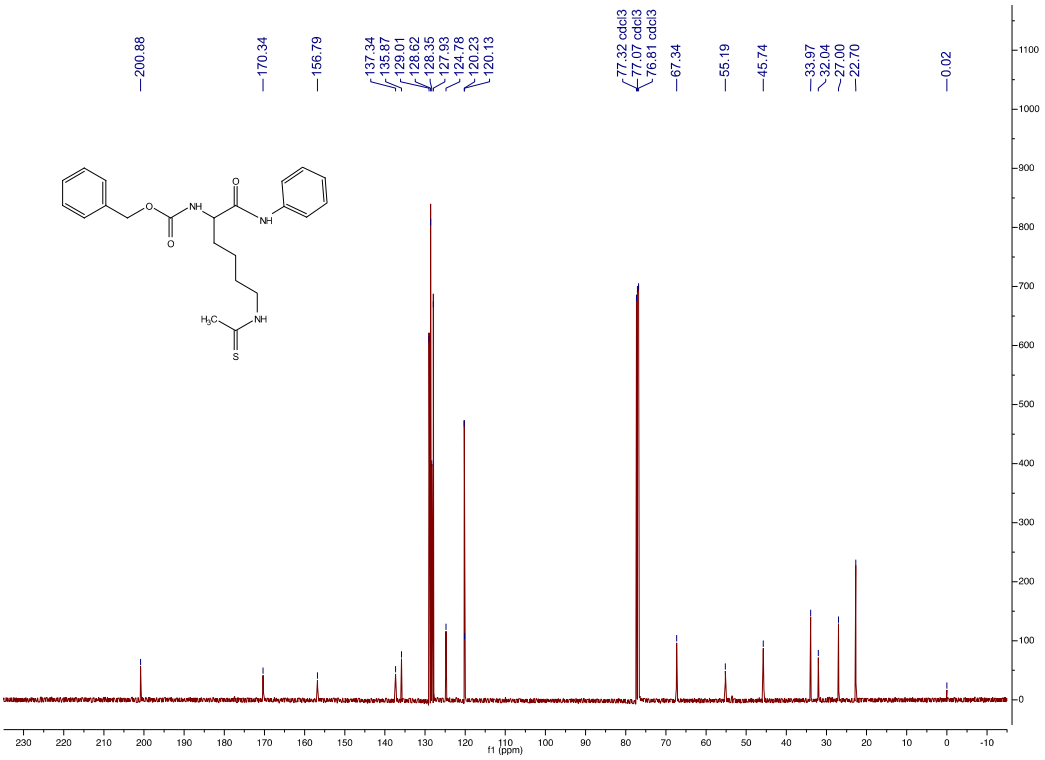

C

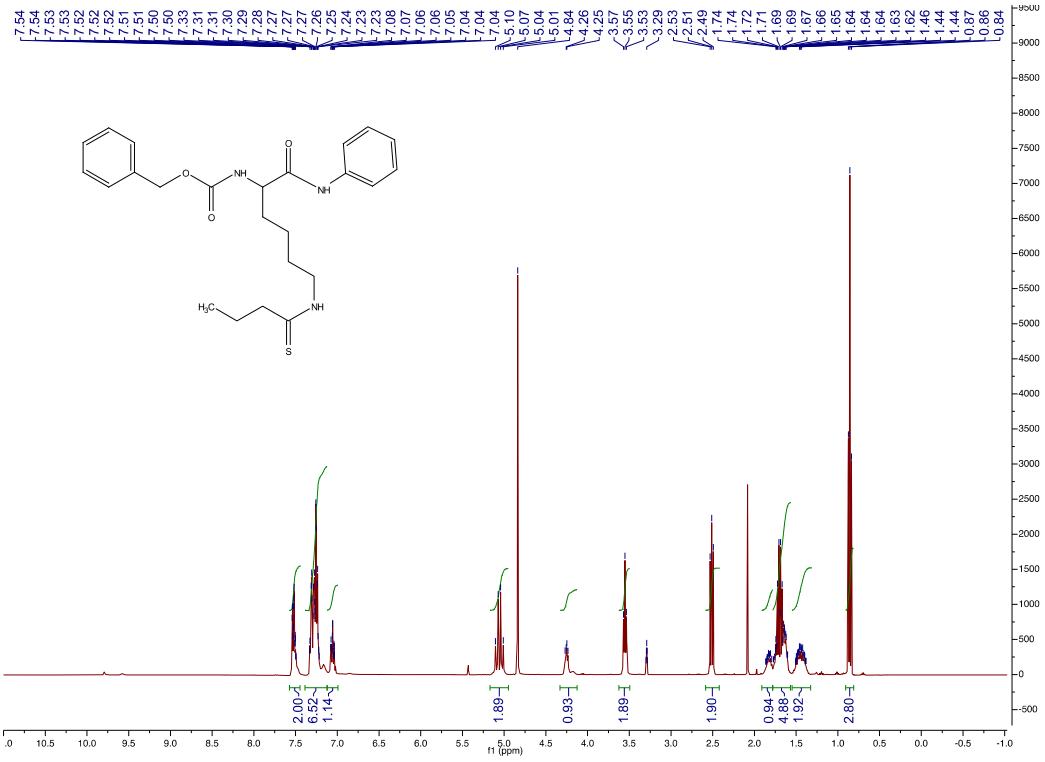

D

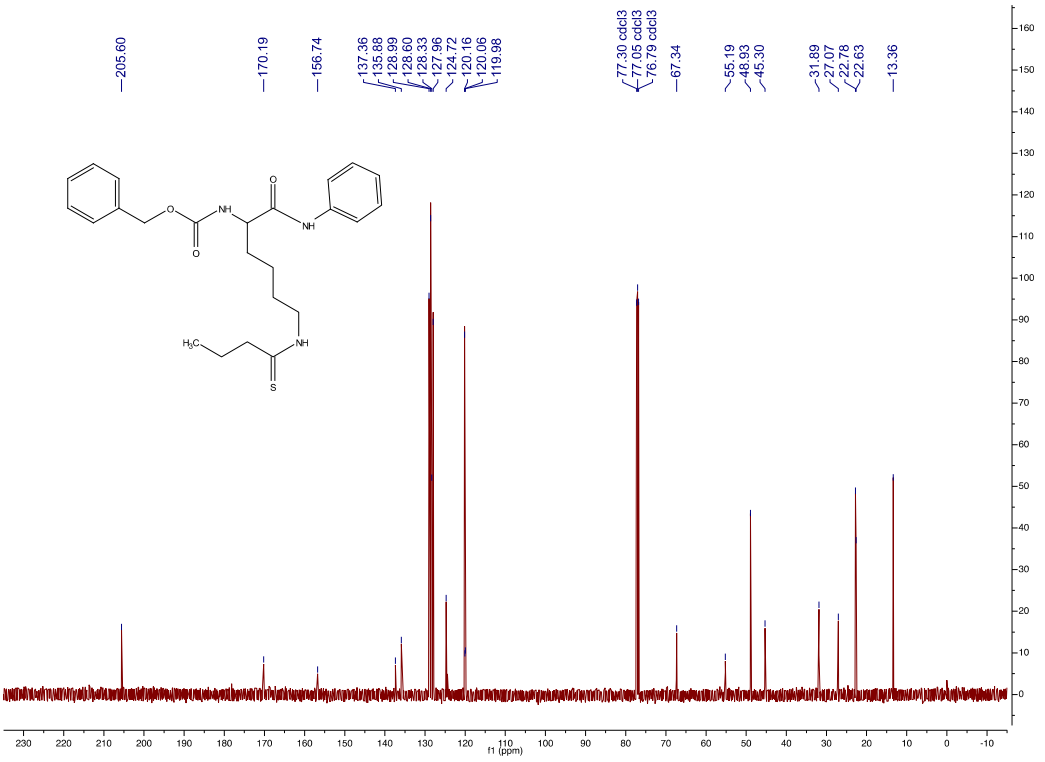

E

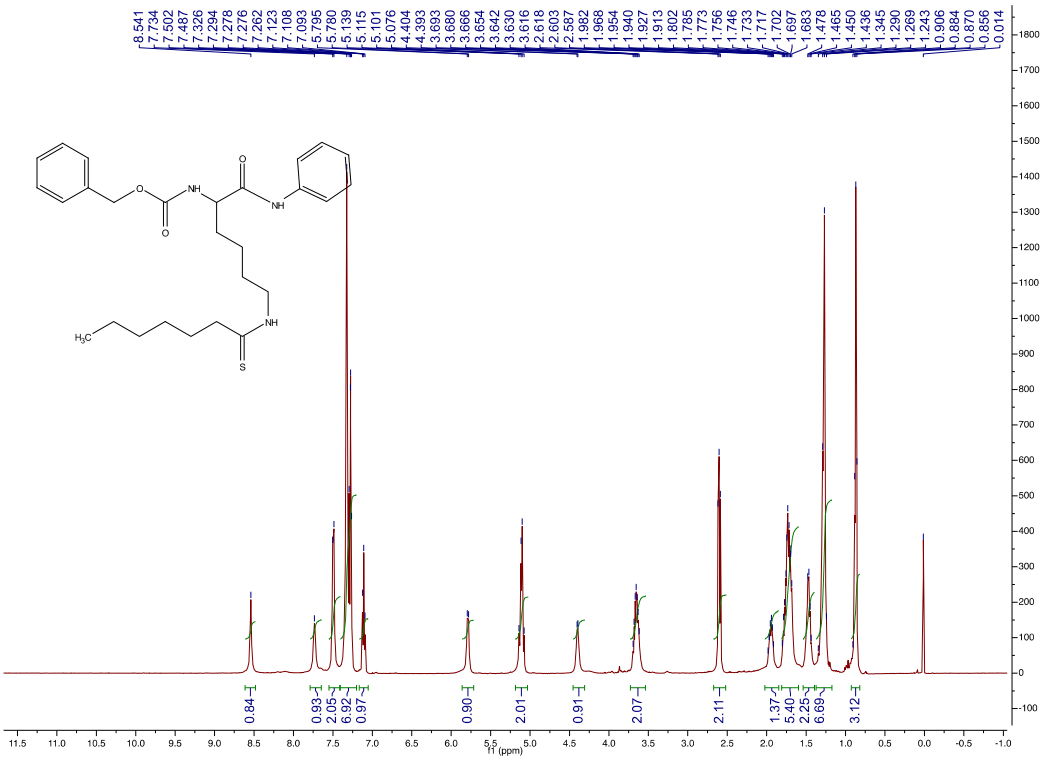
8.541
7.734
7.502
7.487
7.326
7.294
7.278
7.276
7.262
7.123
7.108
7.093
5.795
5.780
5.139
5.115
5.101
5.076
4.404
4.393
3.693
3.680
3.666
3.654
3.642
3.630
3.616
2.618
2.603
2.587
1.982
1.968
1.954
1.940
1.927
1.913
1.802
1.785
1.773
1.756
1.746
1.733
1.717
1.702
1.697
1.683
1.478
1.465
1.450
1.436
1.345
1.290
1.269
1.243
0.906
0.884
0.870
0.856
0.014
0.84
0.93
2.05
6.92
0.97
0.90
2.01
0.91
2.07
2.11
1.37
5.40
2.25
6.69
3.12
H (ppm)

F

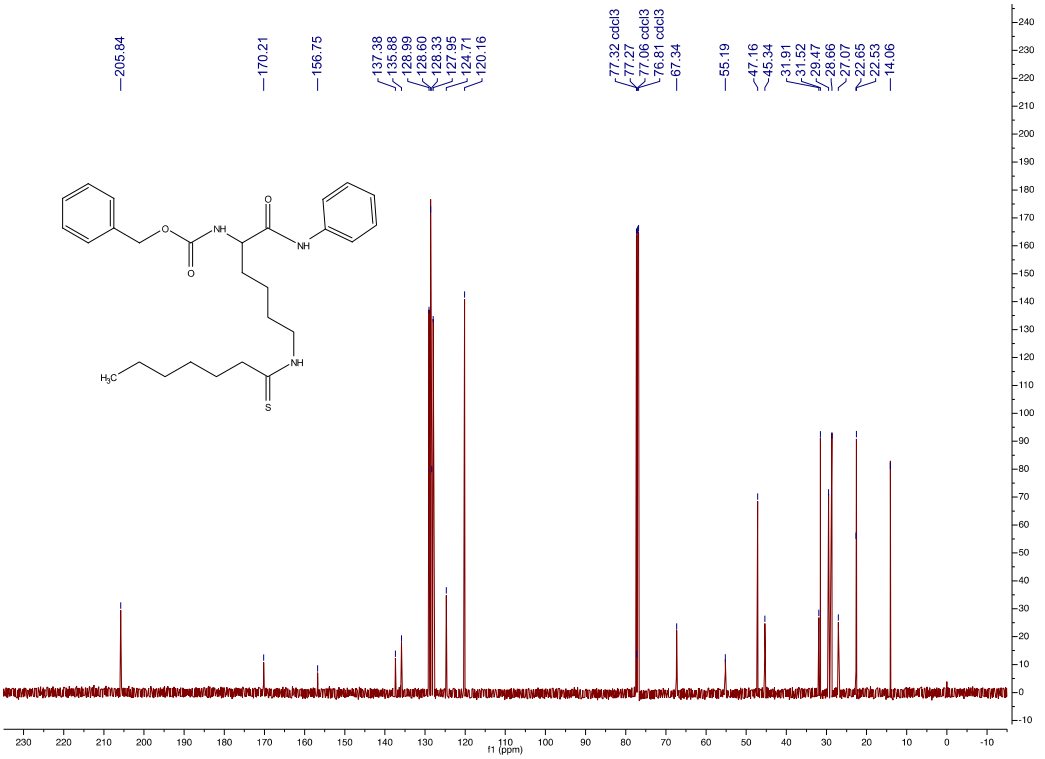
205.84
170.21
156.75
137.38
135.88
128.99
128.60
128.33
127.95
124.71
120.16
77.32 cdcl3
77.27
77.06 cdcl3
76.81 cdcl3
67.34
55.19
47.16
45.34
31.91
31.52
29.47
28.66
27.07
22.65
22.53
14.06
f1 (ppm)

G

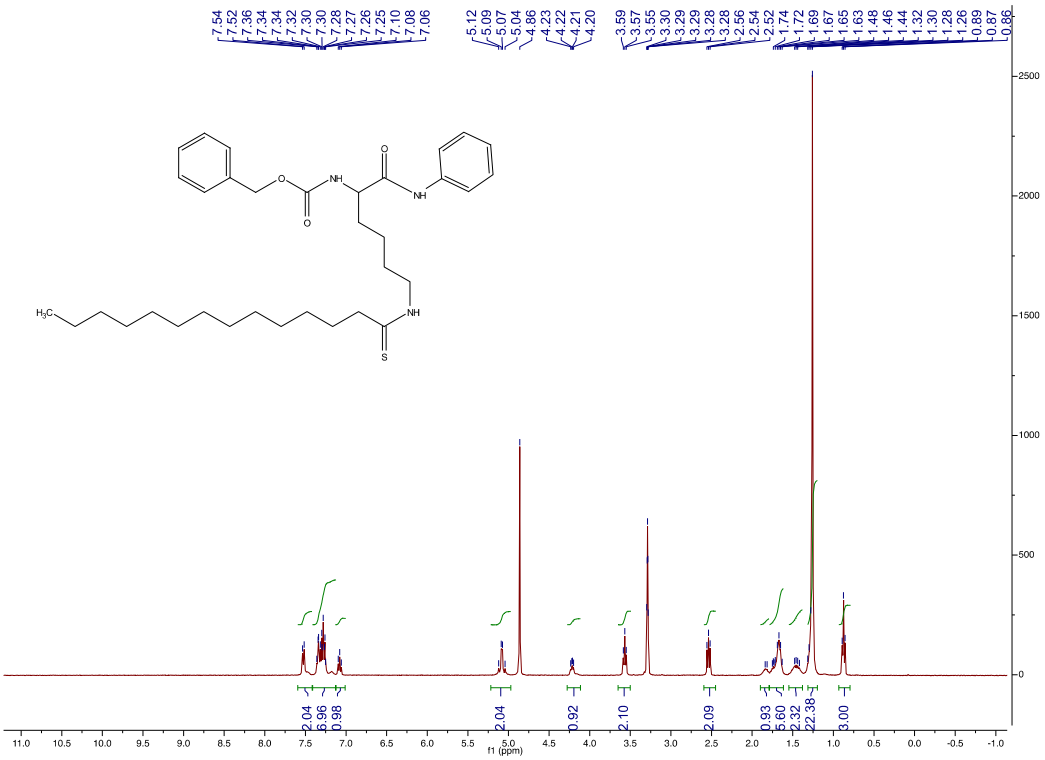
7.54 7.52 7.36 7.34 7.34 7.32 7.30 7.30 7.28 7.27 7.26 7.25 7.10 7.08 7.06
5.12 5.09 5.07 5.04 4.86 4.23 4.22 4.21 4.20
3.59 3.57 3.55 3.30 3.29 3.29 3.28 3.28 2.56 2.54 2.52 1.74 1.72 1.69 1.67 1.65 1.63 1.48 1.46 1.44 1.32 1.30 1.28 1.26 0.89 0.87 0.86
2.04 6.96 0.98 2.04 0.92 2.10 2.09 0.93 5.60 2.32 22.38 3.00
f1 (ppm)

H

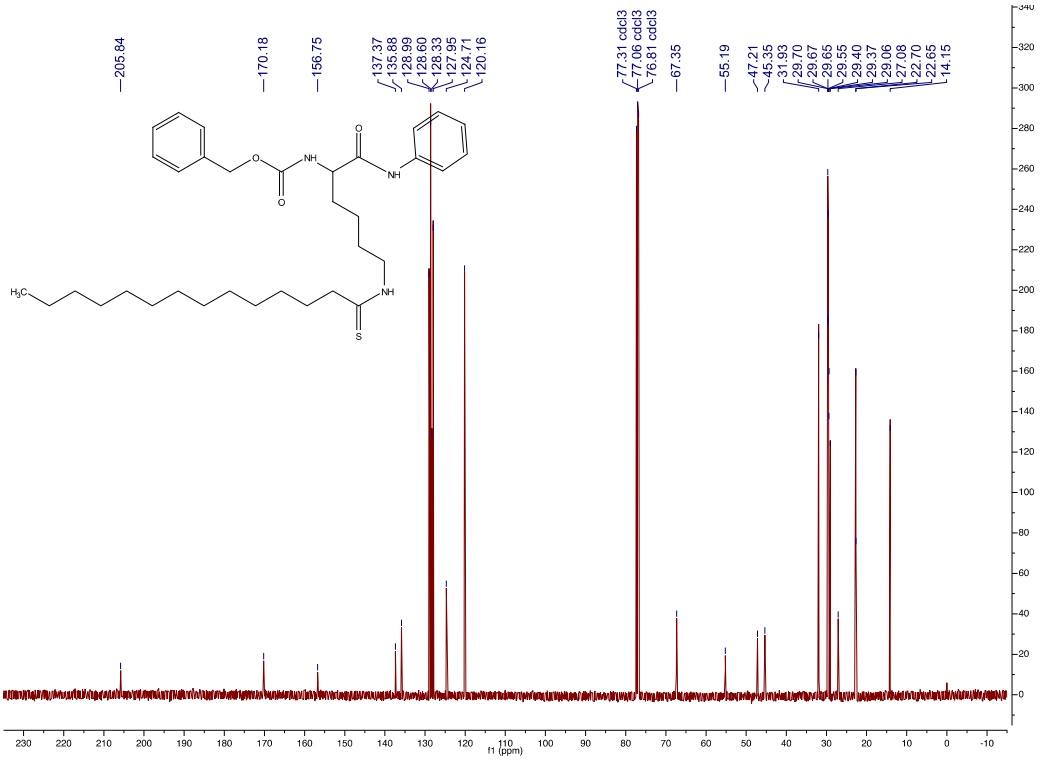
205.84 170.18 156.75 137.37 135.88 128.99 128.60 128.33 127.95 124.71 120.16
77.31 cdcl3 77.06 cdcl3 76.81 cdcl3 67.35 55.19 47.21 45.35 31.93 29.70 29.67 29.65 29.55 29.40 29.37 29.06 27.08 22.70 22.65 14.15
f1 (ppm)

I

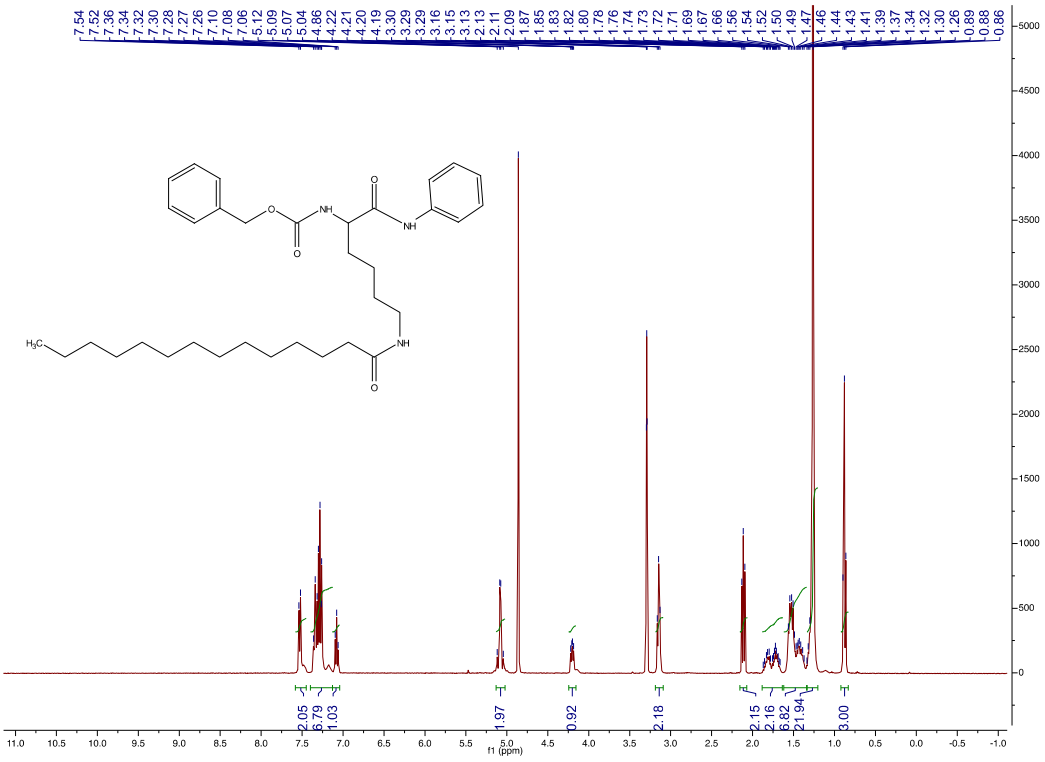
7.54
7.52
7.36
7.34
7.32
7.30
7.28
7.27
7.26
7.10
7.08
7.06
5.12
5.09
5.07
5.04
4.86
4.22
4.21
4.20
4.19
3.30
3.29
3.29
3.16
3.15
3.13
2.13
2.11
2.09
1.87
1.85
1.83
1.82
1.80
1.78
1.76
1.74
1.73
1.72
1.71
1.69
1.67
1.66
1.56
1.54
1.52
1.50
1.49
1.47
1.46
1.44
1.43
1.41
1.39
1.37
1.34
1.32
1.30
1.26
0.89
0.88
0.86
2.05
6.79
1.03
1.97
0.92
2.18
2.15
2.16
6.82
21.94
3.00
f1 (ppm)

J

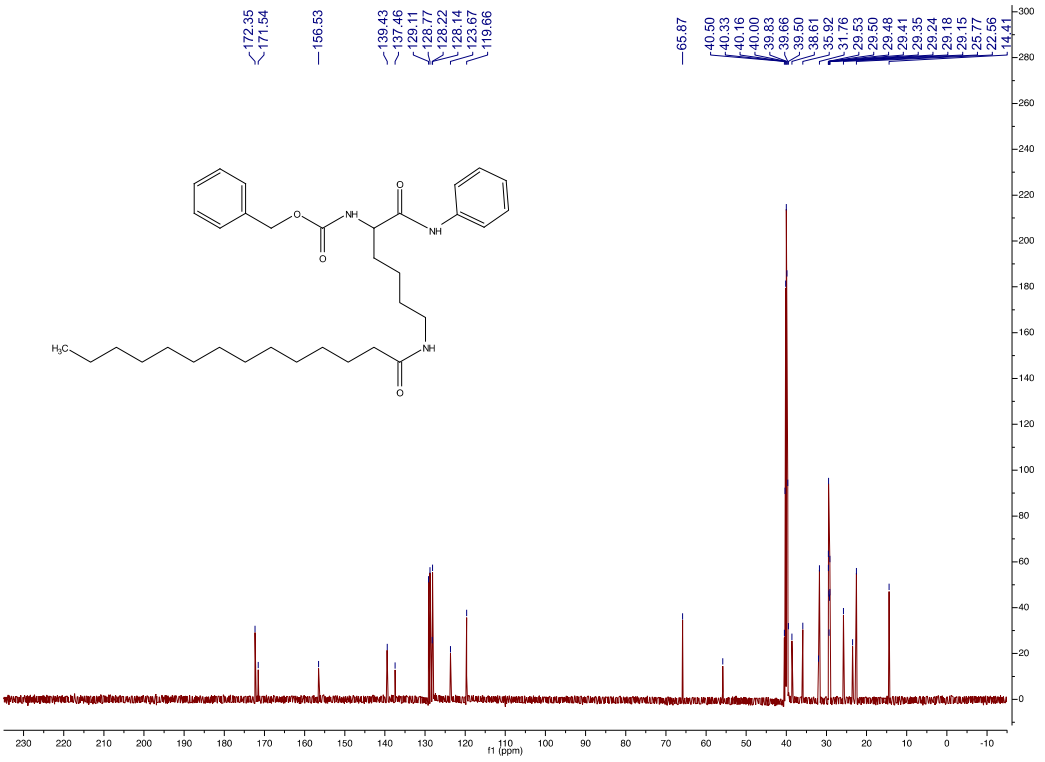
172.35
171.54
156.53
139.43
137.46
129.11
128.77
128.22
128.14
123.67
119.66
65.87
40.50
40.33
40.16
40.00
39.83
39.66
39.50
38.61
35.92
31.76
29.53
29.50
29.48
29.41
29.35
29.24
29.18
29.15
25.77
22.56
14.41
f1 (ppm)

K

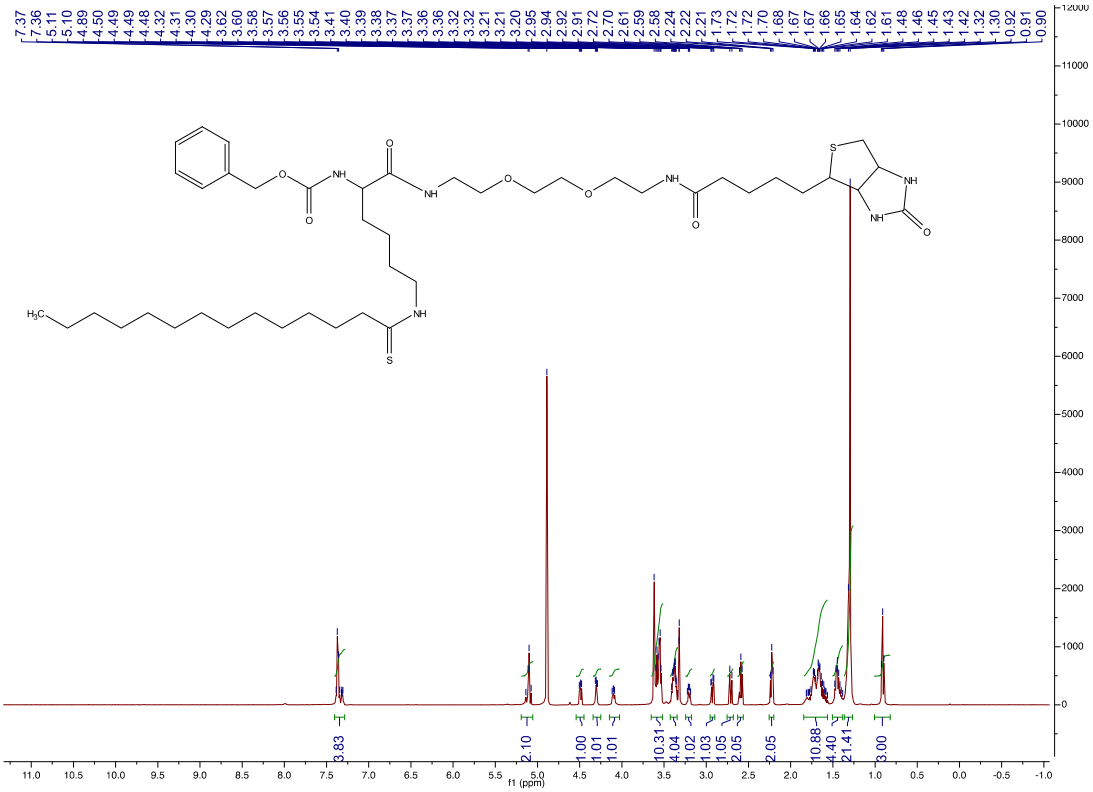
7.37 7.36 5.11 5.10 4.89 4.50 4.49 4.49 4.48 4.32 4.31 4.30 4.29 3.62 3.60 3.58 3.57 3.56 3.55 3.54 3.41 3.40 3.39 3.38 3.37 3.37 3.36 3.36 3.32 3.32 3.21 3.21 3.20 2.95 2.94 2.92 2.91 2.72 2.70 2.61 2.59 2.58 2.24 2.22 2.21 1.73 1.72 1.72 1.70 1.68 1.67 1.67 1.66 1.65 1.64 1.62 1.61 1.48 1.46 1.45 1.43 1.42 1.32 1.30 0.92 0.91 0.90
3.83 2.10 1.00 1.01 1.01 10.31 4.04 1.02 1.03 1.05 2.05 2.05 10.88 4.40 21.41 3.00
f1 (ppm)

L

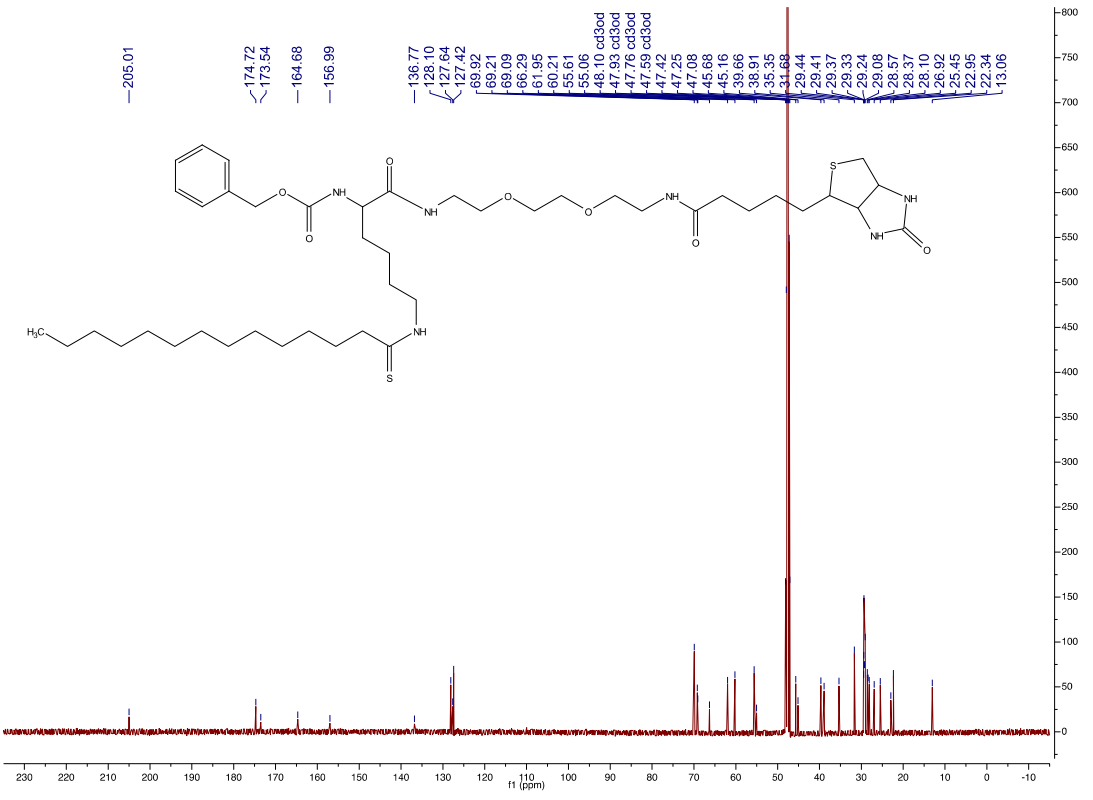
205.01
174.72 173.54 164.68 156.99
136.77 128.10 127.64 127.42
69.92 69.21 69.09 66.29 61.95 60.21 55.61 55.06 48.10 cd3od 47.93 cd3od 47.76 cd3od 47.59 cd3od 47.42 47.25 47.08 45.68 45.16 39.66 38.91 35.35 31.68 29.44 29.41 29.37 29.33 29.24 29.08 28.57 28.37 28.10 26.92 25.45 22.95 22.34 13.06
f1 (ppm)

M

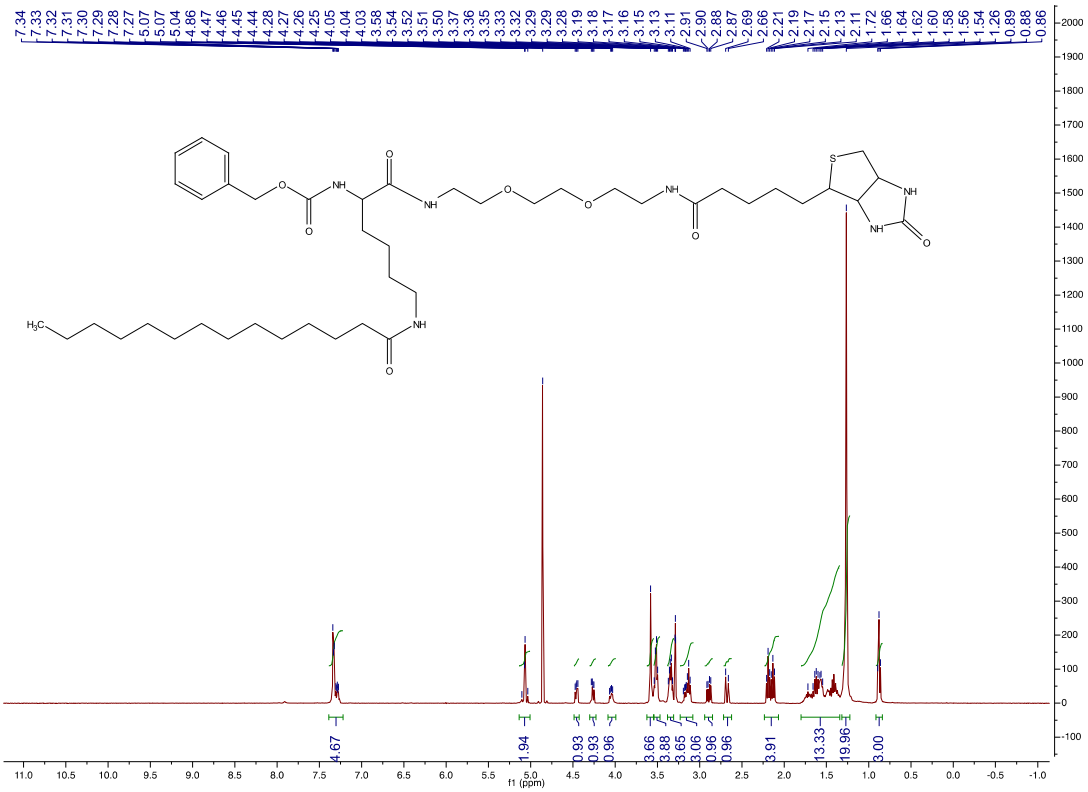

N

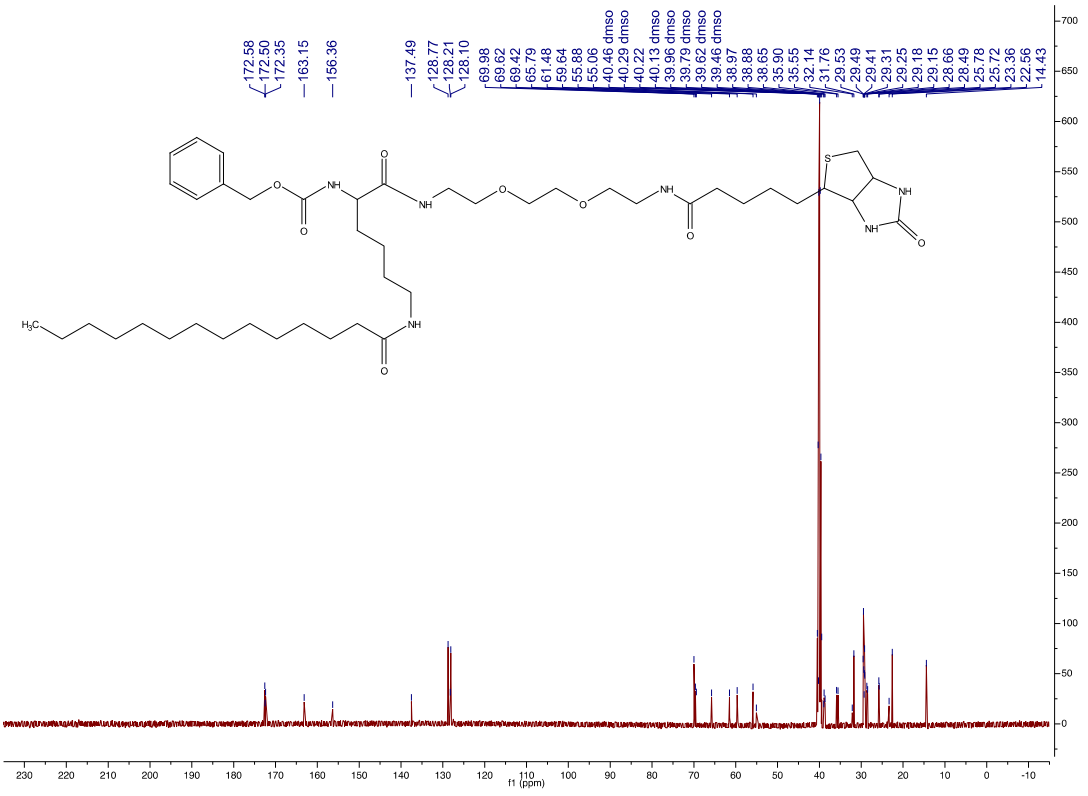

Figure S7. Relate to **Synthesis of Compounds used in the study** in the section of **Experimental Procedures.** NMR spectra of the synthesized compounds. (**A**) ^{1}H NMR spectrum of Compound **TA.** (**B**) ^{13}C NMR spectrum of Compound **TA.** (**C**) ^{1}H NMR spectrum of Compound **TB.** (**D**) ^{13}C NMR spectrum of Compound **TB.** (**E**) ^{1}H NMR spectrum of Compound **TH.** (**F**) ^{13}C NMR spectrum of Compound **TH.** (**G**) ^{1}H NMR spectrum of Compound **TM.** (**H**) ^{13}C NMR spectrum of Compound **TM.** (**I**) ^{1}H NMR spectrum of Compound **M.** (**J**) ^{13}C NMR spectrum of Compound **M.** (**K**) ^{1}H NMR spectrum of Compound **Biotin-TM.** (**L**) ^{13}C NMR spectrum of Compound **Biotin-TM.** (**M**) ^{1}H NMR spectrum of Compound **Biotin-M.** (**N**) ^{13}C NMR spectrum of Compound **Biotin-M.**

Supplemental Experimental Procedures

Cloning, expression and purification of human sirtuins. Human SIRT1, SIRT3, SIRT5 and SIRT6 were expressed as previously described (Du et al., 2009; Jiang et al., 2013). Human SIRT2 (aa38-356) was cloned and inserted into pET28a vector for the expression of N-terminal His6-SUMO fusion protein. Then SIRT2 expression vector was introduced into an *E. coli* BL21. Successful transformation were selected by plating the cells on kanamycin (50 μg mL^{-1}) and chloramphenicol (20 μg mL^{-1}) luria broth (LB) plates. Single colonies were selected and grown in LB with kanamycin (50 μg mL^{-1}) and chloramphenicol (20 μg mL^{-1}) overnight at 37 °C. On the following day the cells were subcultured (1:1000 dilution) into 2 L of LB with kanamycin (50 μg mL^{-1}) and chloramphenicol (20 μg mL^{-1}). The cells were induced with 20 μM of isopropyl β-D-1-thiogalactopyranoside (IPTG) at an OD_{600} of 0.6 and grown overnight at 15 °C, 200 rpm. The cells were harvested by centrifugation at 8000 rpm for 5 min at 4 °C (Beckman Coulter refrigerated floor centrifuge) and passed through an EmulsiFlex-C3 cell disruptor (AVESTIN, Inc.) 3 times. Cellular debris was removed by centrifuging at 20,000 rpm for 30 min at 4 °C (Beckman Coulter). The supernatant was loaded onto a nickel column (Histrap, Ge Healthcare) pre-equilibrated with 20 mM Tris-HCl pH 8.0 with 500 mM NaCl. The protein was eluted with a linear gradient of imidazole (0-500 mM). The desired fractions were pooled, concentrated and buffer exchanged. The His6-SUMO tag was removed by overnight incubation at 4 °C with ULP1, followed by Ni-affinity column purification to remove any undigested SIRT2. The tag-free SIRT2 was further purified on a Superdex 75 column (Bio-Rad, Hercules, CA). The protein was eluted with 20 mM Tris-HCl, pH 8.0, 500 mM NaCl. After concentration, the target protein was frozen at -80 °C.

Reagents, antibodies and plasmids. All chemicals were obtained in the highest purity available. MG132 was from Cayman Chemical Co. (Ann Arbor, MI). Cycloheximide was purchased from Amresco (Euclid, OH). Trichostatin A (TSA) and AGK2 (2-Cyano-3-[5-(2,5-dichlorophenyl)-2-furanyl]-N-5-quinolinyl-2-propenamide) were obtained from Sigma-Aldrich (St. Louis, MO).

The anti-human SIRT1 antibody (3H10.2) was from EMD Chemicals Inc. (San Diego, CA). The anti-human SIRT2 (EPR1667), SIRT6 antibodies were from Abcam (Cambridge, MA). The anti-

human SIRT3 (C73E3), acetyl-p53 (Lys382) antibodies were obtained from Cell Signaling Technology (Danvers, MA). The anti-SIRT7 (C-3), c-Myc (9E10), NEDD4 (H-135), ubiquitin (P4D1), β-actin (C4) and the goat anti-mouse/rabbit IgG-horseradish peroxidase-conjugated antibodies were purchased from Santa Cruz Biotechnology (Santa Cruz, CA). The anti-SIRT4 (LS-C100490) antibody was purchased from LSBio, Inc. (Seattle, WA). The anti-SIRT5 antibody (Center) was from Abgent (San Diego, CA). The anti-acetyl-α-tubulin (6-11B-1), α-tubulin (B-5-1-2) antibodies, the anti-Flag M2 antibody conjugated with horseradish peroxidase and the anti-Flag M2 affinity gel were from Sigma-Aldrich.

The pLKO.1-puro lentiviral shRNAs constructs toward Luciferase and SIRT1-7 were purchased from Sigma-Aldrich. Luciferase shRNA (SHC007), SIRT1 shRNA1 (TRCN0000018980), SIRT1 shRNA2 (TRCN0000018981), SIRT2 shRNA1 (TRCN0000040221), SIRT2 shRNA2 (TRCN0000310335), SIRT3 shRNA1 (TRCN0000038890), SIRT3 shRNA2 (TRCN0000038893), SIRT4 shRNA1 (TRCN0000018948), SIRT4 shRNA2 (TRCN0000232894), SIRT5 shRNA1 (TRCN0000018544), SIRT5 shRNA2 (TRCN0000018545), SIRT6 shRNA 1 (TRCN0000378253) and shRNA 2 (TRCN0000232528), SIRT7 shRNA1 (TRCN0000359663), and SIRT7 shRNA2 (TRCN0000020254) were used. The scrambled siRNA and Stealth Select RNAi™ siRNA targeting SIRT2 (HSS117928 and HSS177042) were purchased from Invitrogen (Carlsbad, CA). To generate human SIRT2 with C-terminal Flag-tag expression vector, full-length human *SIRT2* cDNA was amplified by PCR and inserted into pCMV-tag-4a vector between BamHI and XhoI sites. A human c-Myc expression vector with N-terminal Flag-tag was obtained by PCR amplification of *Flag-c-Myc* and subcloning via BamHI and XhoI sites into pCMV-tag-4a vector.

Inhibition assay for SIRT1, SIRT2, SIRT3, SIRT5. Different concentrations (0.0064, 0.032, 0.16, 0.8, 4.0, 20, 100 and 200 μM) of TA~TM, and M were pre-incubated with 0.1 μM of SIRT1, 0.2 μM of SIRT2, 1 μM of SIRT3 or 1 μM of SIRT5, respectively, and 1 mM NAD in 20 mM Tris-HCl buffer (pH 8.0) with 1 mM dithiothreitol (DTT) at 37 °C for 15 min. Then 10 μM of acyl peptide (acetyl-H3K9 for SIRT1, SIRT2 and SIRT3; succinyl-H3K9 for SIRT5) was added to initiate the reactions. Then reactions were incubated at 37°C in a total volume of 60 μL (5 min for SIRT1, 5 min for SIRT2, 20 min for SIRT3, and 10 min for SIRT5). The reactions were stopped by adding 60 μL of an aqueous solution of 50% methanol containing 200 mM HCl and 320 mM acetic acid.

After quenching the sirtuin reactions, centrifugation was used to remove precipitated proteins and the supernatant was analyzed by HPLC with a reverse phase C18 column (Kinetex XB-C18 100A, 100 mm × 4.60 mm, 2.6 μm, Phenomenex) with a gradient of 0 % in 2 min, 0% to 20% in 2min, 20% to 40% B in 13 min and then 40% to 100% for 2 min at 0.5 mL/min. Product quantification was based on the area of absorbance monitored at 280 nm. The peak areas were integrated and the conversion rate was calculated from the peak areas as the fraction of the free H3K9 peptide from the total peptide.

All reactions were done in duplicate.

Determination of kinetic parameters for TM. For SIRT2 inhibition kinetics of TM, a mixture of acetyl-H3K9 (acH3K9) peptide substrate (2.5, 5, 10, 25, 50, 100, 187.5 μM), NAD (25, 50, 100, 250, 500, 1000, 1500 μM), TM (0, 0.01, 0.03, 0.1, and 0.3 μM), 20 mM Tris-HCl (pH 8.0) and 1 mM DTT was incubated at 37 °C. 1 mM NAD was used for determining the kinetic parameters for acH3K9 peptide, 100 μM of acH3K9 peptide was used for the determination of kinetic parameters for NAD. The reaction was started by adding 0.2 μM of SIRT2, and stopped after 5 min by adding 60 μL of an aqueous solution of 50% methanol containing 200 mM HCl and 320 mM acetic acid. The samples were analyzed by HPLC as described above and the initial velocity was calculated. The K_m and v_{max} were obtained from Michaelie-Menten plots using Graphpad Prism software.

Mass spectrometry detection of the stalled intermediate formed by TM and NAD. Reactions containing 50 μM SIRT2, 100 μM NAD, 100 μM TM, 1 mM DTT, and 20 mM pyridinium formate (pH 7.0) was reacted for 5 min at 37 °C. Controls were run in which NAD or SIRT2 was removed from the reaction mixture. Reactions were quenched with 1 volume of acetonitrile and the mixture was centrifuged to remove the precipitated protein. The supernatant was then analyzed by LC-MS using water and acetonitrile as solvents.

Inhibition assay for SIRT6. Different concentrations (0.0125, 0.05, 0.2, 0.8, 3.2, 12.8, 51.2, 204.8 μM) of TA~TM were pre-incubated with 1 μM of SIRT6 and 1 mM NAD in 20 mM Tris-HCl buffer (pH 8.0) with 1 mM DTT at 37°C for 20 min. Then 50 μM of myristoyl-H3K9 peptide (myrH3K9) was added to initiate the reactions. The reactions were incubated at 37 °C in a total volume of 60 μL for 1 hr. The reactions were stopped by adding 60 μL of an aqueous solution of 50% methanol containing 200 mM HCl and 320 mM acetic acid.

Inhibition assay for SIRT7. Different concentrations (0.0125, 0.05, 0.2, 0.8, 3.2, 12.8, 51.2, 204.8 μM) of TA~TM were pre-incubated with 1 μM of SIRT7 and 1 mM NAD in 150mM NaCl and 50 mM KH_2PO_4 buffer (pH 8.0) with 1 mM DTT at 37°C for 20 min. Then 10 μM myrH3K9 peptide and 0.083mg/mL tRNA were added to initiate the reactions. Then reactions were incubated at 37 °C in a total volume of 60 μL for 110 min. The reactions were stopped by adding 60 μL of an aqueous solution of 50% methanol containing 200 mM HCl and 320 mM acetic acid.

Cell culture and transfection. All cell culture media contained 10% (vol/vol) heat-inactivated fetal bovine serum (FBS; Invitrogen, Carlsbad, CA) and 1% penicillin-streptomycin (Invitrogen) unless otherwise specified. Human MCF-7, MDA-MB-231, MDA-MB-468, HeLa, HME1 cells were grown in DMEM media (Invitrogen). Human BT-549, SK-BR-3, MDA-MB-453 and K562 cells were grown in RPMI-1640 media (Invitrogen). The MCF-10A cells were cultured in mammary epithelial cell growth medium (MEGM; Lonza, Walkersville, MD) with supplements according to

manufacturer's instruction.

To overexpress SIRT2 or c-Myc in cells, the pCMV-tag-4a vector containing *SIRT2* or *c-Myc,* or pCDH vector containing *c-Myc* were transfected into cells using FuGene 6 (Promega, Madison, WI) according to manufacturer's protocol. Empty vector was transfected as negative control.

Soft agar colony formation assay. For colony formation in semisolid medium, 1.0×10^4 cells were plated in 0.3% low-melting point agarose (LMP, Invitrogen) onto 6-well plate coated with 1.2% LMP mixed with 2 × complete medium. For treatments, 2 × inhibitor was added to cells at the time of plating. The medium and inhibitor were replaced with fresh ones every 3 days. For colony formation of the SIRT2 KD cells, cells were transfected with the scrambled siRNA or SIRT2 siRNAs for 48 hr before plating in 6-well plate. Similarly, cell media was replaced every 3 days. After 14 days of incubation, colonies were photographed and counted with ImageJ.

Western blot analysis. Western blot analysis was performed as described previously (Jiang et al., 2013). The proteins of interest were detected using enzyme-linked chemiluminescence (ECL; Pierce Biotechnology Inc.) and visualized using the Storm Imager (GE Healthcare, Piscataway, NJ). Quantification of Western blots was done using the Quantity One software (Bio-Rad).

Biotin-TM/M pull-down assay. HEK293T cells were collected and lysed in lysis buffer containing 25 mM Tris, pH 7.4, 150 mM NaCl, 10% glycerol, 1% Nonidet P-40 and 1 × protease inhibitor cocktail (Sigma-Aldrich). The cell extract supernatant was collected after centrifugation at 14,000 g for 20 min at 4 °C. Cell lysates were incubated with 10 μM Biotin-TM or Biotin-M in the absence or presence of 1 mM NAD at 4 °C for 1 hr. The high capacity streptavidin resin (Pierce Biotechnology, Rockford, IL) was added to the mixture and incubated at 4 °C for another 1 hr. After centrifugation at 500 g for 2 min at 4 °C, the streptavidin resin was washed 3 times with 1 mL washing buffer (25 mM Tris, pH 7.4, 150 mM NaCl, 10% glycerol, 0.2% Nonidet P-40). The resin-bound proteins were then separated with SDS-PAGE and immunoblotted with anti-SIRT1 or anti-SIRT2 antibodies.

To assess the binding of TM to SIRT2 in cells, MCF-7 parental cells, Luciferase KD and SIRT2 KD cells were treated with 50 μM D-Biotin or Biotin-TM as indicated for 6 hr and then lysed in lysis buffer containing 1 mM NAD. Cell extract was collected, streptavidin pull-down and western blot analysis was performed as described above.

SIRT1 inhibition in cells. MCF-7 or MDA-MB-468 cells were treated with indicated test compounds in the presence of 200 nM TSA for 6 hr. The acetylation level of p53 protein was determined by western blot using anti-acetyl-p53 (K382) antibody. β-actin served as a loading control.

SIRT2 inhibition in cells. MCF-7 cells were treated with indicated inhibitors at for 6 hr after

being transfected with pCMV-tag-4a-*SIRT2* for 18 hr. Cells were collected and lysed in lysis buffer containing 25 mM Tris, pH 7.4, 150 mM NaCl, 10% glycerol, 4 mM $MgCl_2$, 0.2 mM DTT, 100 mM NAD, 1% Nonidet P-40 and 1 × protease inhibitor cocktail. And the cell lysates were subjected to western blot for the analysis of acetyl-α-tubulin (K40) and α-tubulin levels.

TM treatment of mice bearing human breast cancer xenotransplants. Two million MDA-MB-231 cells suspended in 100 μL 1 × PBS and 100 μL Matrigel were injected subcutaneously on the flanks of female Ncr Nu/Nu mice. Following the injections, mice were permitted to recover and monitored biweekly, including tumor measurement using calipers. Once the majority of tumors reached a threshold size of 200 mm^3, mice with intraperitoneal (IP) or intra-tumor (IT) injections of vehicle alone (DMSO) or inhibitor (TM in DMSO) over one month. IP injections of 1.5 mg TM in 50 μL DMSO were given daily. IT injections of 0.75 mg TM in 50 μL DMSO per tumor were given 3 days per week. After one month of treatment or if mice met humane endpoint criteria, mice were euthanized by CO_2 asphyxiation. Tissues were collected, fixed with 10% neutral-buffered formalin, embedded in paraffin, sectioned, and stained with hematoxylin and eosin (H&E). H&E-stained sections were scanned using an Aperio ScanScope and analyzed by a veterinarian certified in anatomic pathology by the American College of Veterinary Pathologists blinded to treatment group. Serum, tumor tissues and organs were snap frozen in liquid N_2 and stored at -80 °C for subsequent analyses.

TM treatment of MMTV-*PyMT* mice. MMTV-*PyMT* transgenic female mice on a pure FVB/N background were obtained from the Jackson Laboratory and treated beginning at 6 weeks of age with daily IP injections of vehicle (DMSO) or 1.5 mg TM in 50 μL DMSO over one month. Mice were monitored daily for tumor development and health status, and tumor size was measured twice per week. After one month of treatment or if mice met humane endpoint criteria, mice were euthanized by CO_2 asphyxiation and necropsied. Tissues were collected and analyzed as described above.

Ubiquitination assay. MCF-7 cells were transfected with pCMV-tag-4a or pCMV-tag-4a-*c-Myc*, respectively. 18 hours after transfection, cells were treated with 25 μM TM for 6 hr in the presence of proteasome inhibitor MG132 (10 μM). Immunoprecipitation was performed with the cell lysates by anti-Flag M2 affinity gel as described previously (He et al., 2014). The gel-bound proteins were resolved on SDS-PAGE and detected with anti-ubiquitin antibody. The c-Myc level in total cell lysates was used as input control.

Reverse transcription (RT)-PCR analysis of mRNA levels. Total RNA was extracted from vehicle-, TM- or M-treated cells using RNeasy Mini Kit (Qiagen, CA, USA) according to the manufacturer's instructions. The concentration and purity of total RNA were determined by using the NanoDrop (Thermo Fisher Scientific Inc, Wilmington, DE). cDNA was synthesized using SuperScript

III reverse transcriptase (Invitrogen). Amplification of genes of interest was performed using Herculase II Fusion DNA Polymerase (Agilent Technologies, Santa Clara, CA) with the gene-specific primers shown below. 10 µl of each PCR product were analyzed by gel electrophoresis on a 2% agarose gel.

Primer target	Direction	Sequence
c-Myc	Forward	GGCTCCTGGCAAAAGGTCAGAGT
c-Myc	Reverse	CTGCGTAGTTGTGCTGATGTGT
NEDD4	Forward	TCAGGACAACCTAACAGATGCT
NEDD4	Reverse	TTCTGCAAGATGAGTTGGAACAT
Actin	Forward	CATGTACGTTGCTATCCAGGC
Actin	Reverse	CTCCTTAATGTCACGCACGAT
STUB1	Forward	AGCAGGGCAATCGTCTGTTC
STUB1	Reverse	CAAGGCCCGGTTGGTGTAATA
SKP2	Forward	ATGCCCCAATCTTGTCCATCT
SKP2	Reverse	CACCGACTGAGTGATAGGTGT
TRPC4AP	Forward	ACAAGCACACGCTTCTTGC
TRPC4AP	Reverse	CTGACACCTTTCGAGTCGCC
FBXW7	Forward	CGACGCCGAATTACATCTGTC
FBXW7	Reverse	CGTTGAAACTGGGGTTCTATCA
FBXO32	Forward	GCCTTTGTGCCTACAACTG
FBXO32	Reverse	CTGCCCTTTGTCTGACAGAAT

Immunofluorescence of cultured cells. MDA-MB-231 cells were treated with ethanol, M (25 µM) or TM (25 µM) for 6 hr. Immunostaining was performed and images were acquired by confocal microscopy as previously described (Mabjeesh et al., 2003).

Flow cytometry. For cell cycle analyses, MCF-7 or K562 cells were treated with 25 µM for 0, 24, 48 and 72 hr. Cells were spun down, washed with PBS, fixed with 70% ethanol overnight, and then washed with PBS. RNA was degraded with RNAse A and DNA was stained with propidium iodide (Invitrogen). Samples were analyzed on a BD LSR-II. Cell cycle analysis was performed with FlowJo flow cytometry analysis software (Tree Star, Inc., Ashland, OR).

Cellular senescence staining. MCF-7 or K562 cells were treated with ethanol or 25 µM TM. After 5 days of treatment, cells were stained for senescence as previously described (Debacq-Chainiaux et al., 2009).

Immunofluorescence and Immunohistochemistry of tumor sections. Formalin-fixed, paraffin-embedded (FFPE) tumors were sectioned, dewaxed and submitted to heat mediated antigen retrieval in 0.01 M citrate buffer for 50 min. For immunofluorescence, sections were incubated with anti-acetyl-α-tubulin, followed by Alexa Fluro-488 conjugated secondary antibodies from Invitrogen and cell nuclei counterstaining with DAPI Fluoromount-G® from SouthernBiotech. Fluorescent

images were taken using Zeiss LSM880 inverted confocal microscopy (Carl Zeiss Inc., Thornwood, NY). For immunohistochemistry, sections were incubated with anti-Ki67 Clone MM1 (Vector Laboratories) antibody followed by biotinylated polyclonal rabbit anti-mouse (DAKO). Color was developed using 3,3'-Diaminobenzidine tetrahydrochloride substrate from Invitrogen and counterstained with hematoxilin. Images were scanned using an Aperio ScanScope.

Synthesis of compounds used in the study

General methods. Reagents were obtained from Aldrich or Acros in the highest purity available and used as supplied. ^{1}HNMR was performed on INOVA 400/500 spectrometer. LCMS was carried out on a SHIMADZU LC and Thermo LCQ FLEET MS with a Sprite TARGA C18 column (40 × 2.1 mm, 5 μm, Higgins Analytical, Inc.) monitoring at 215 and 260 nm. Solvents used in LCMS were water with 0.1% acetic acid and acetonitrile with 0.1% acetic acid.

1. Synthetic Route for TA

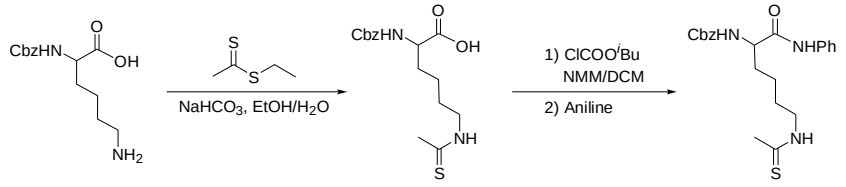

1 2 TA

Synthesis of compound 2. To a solution of Z-Lys-OH (2.8 g, 10 mmol) in ethanol (100 mL) was added 20 mL of 10% (w/v) Na_2CO_3 aqueous solution at 0°C. The reaction mixture was allowed to warm to room temperature (rt) while stirred extensively. Ethyl dithioacetate (1.32 g, 11 mmol) was added and the reaction mixture was stirred overnight at rt. Solvent was evaporated and then the crude product was acidified to pH **=** 2 with 3 M HCl on ice and extracted with DCM (3 x 100 mL). The organic phase was washed with brine (2 x 30 mL), dried with Na_2SO_4, and evaporated to obtain compound **2,** which was directly used in the next step without further purification.

Synthesis of compound TA. To a solution of compound **2** (3.38 g, 10 mmol) and N-methylmorpholine (1.1 ml, 10 mmol) in dry dichloromethane (100 mL) at 0°C was added dropwisely iso-butylchloroformate (1.3 ml, 10 mmol). The reaction mixture was stirred for 30 min at 0°C. Aniline (1.09 ml, 12 mmol) was added at 0°C and the reaction mixture was stirred overnight at room temperature. The solvent was removed under reduced pressure and the resulting residue was purified by flash chromatography on silica gel (Hexane/ethyl acetate = 2/1) to afford the expected compound **3** (3.95 g, 95.5% yield). ^{1}H NMR (400 MHz, CD_3OD): δ 7.53-7.51 (m, 2H), 7.34-7.22 (m, 7H), 7.08-7.04(t, *J* =7.2Hz, 1H), 5.06 (q, *J*=8.0Hz, 2H), 4.26-4.22 (m, 1H), 3.54 (t, *J*=7.1Hz, 2H), 2.39 (s, 3H), 1.89-1.76(m, 1H), 1.78-1.70 (m, 1H), 1.66-1.58 (m, 2H), 1.55-1.35 (m, 2H). ^{13}C NMR (126 MHz, $CDCl_3$): δ 200.88, 170.34, 156.79, 137.34, 135.87, 129.01, 128.62, 128.35, 127.93, 124.78, 120.23, 120.13, 67.34, 55.19, 45.74, 33.97, 32.04, 27.00, 22.70.LCMS (ESI) calcd. for C22H28N3O3S $[M+H]^+$ 414.2, obsd. 414.3.

2. Synthetic Route for TB, TH, and TM

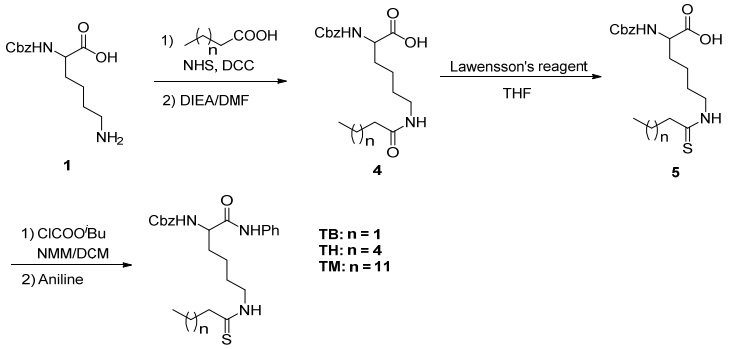

Synthesis of compound 4. To the solution of acid (30 mmol) in anhydrous *N, N'*-dimethylformamide (DMF, 20 mL) was added *N*-hydroxysuccinimide (NHS, 3.45 g, 30 mmol) with stirring at rt. Then *N, N'*-dicyclohexylcarbodiimide (DCC, 6.19 g, 30 mmol) in anhydrous DMF (20 mL) was added to the reaction. After stirring for 2 hr, the reaction mixture was filtered. The filtrate was added to a solution of Z-Lys-OH (8.4 g, 30 mmol) with *N, N*-diisopropylethylamine (DIEA, 5.2 mL, 30 mmol) in anhydrous DMF (50.0 mL) at room temperature. The resulting reaction mixture was stirred overnight. Then 44 mL water and 26 mL 1 M HCl was added to the reaction mixture to adjust pH to 2~3. The mixture was extracted ethyl acetate (3 x 200 mL) and washed brine (2 x 100 mL). The organic layer was dried over anhydrous sodium sulfate. After removal of the solvents in vacuum, the residue was purified by flash chromatography on silica gel (DCM/MeOH = 20:1) to afford the expected compound **4** (85% yield).

Synthesis of compound 5. To a solution of compound **4** (20 mmol) in THF (100 mL) was added Lawesson's reagent (8.0 g, 20 mmol) at room temperature. The reaction mixture was stirred overnight under nitrogen (monitored by LCMS). After removal of THF using a rotary evaporator, the residue was purified by silica gel column (DCM/MeOH = 20:1) to give the product as a white solid (76% yield).

Synthesis of compound TB, TH and TM. To a solution of compound **5** (10 mmol) and N-methylmorpholine (1.1 ml, 10 mmol) in dry dichloromethane (100 mL) at 0°C was added dropwisely iso-butylchloroformate (1.3ml, 10 mmol). The reaction mixture was stirred for 30 min at 0°C. Aniline (1.09 ml, 12 mmol) was then added at 0°C and the reaction mixture was stirred overnight at room temperature. The solvent was removed under reduced pressure and the resulting residue was purified by flash chromatography on silica gel (Hexane/ethyl acetate= 2/1) to afford the expected compound **TB, TH, and TM**.

TB (91% yield) ^{1}H NMR (400 MHz, CD_3OD): δ 7.57-7.45 (m, 2H), 7.39-7.12 (m, 7H), 7.12-6.99 (m, 1H), 5.05 (q, *J* = 12.5 Hz, 2H), 4.27-4.23 (m, 1H), 3.55 (q, *J* = 12.5 Hz, 2H), 2.51 (t, *J* = 7.2Hz, 2H), 1.91-1.78 (m, 1H), 1.78-1.57 (m, 5H), 1.55-1.33 (m, 2H), 0.86 (t, *J* = 7.2 Hz, 3H).. ^{13}C NMR (126 MHz, $CDCl_3$): δ 205.60, 170.19, 156.74, 137.36, 135.88, 128.99, 128.60, 128.33, 127.96, 124.72, 120.16, 120.06, 119.98, 67.34, 55.19, 48.93, 45.30, 31.89, 27.07, 22.78, 22.63, 13.36. LCMS (ESI) calcd. for C24H32N3O3S $[M+H]^+$ 442.2, obsd. 442.3;

TH (89% yield) ^{1}H NMR (500 MHz, $CDCl_3$): δ 8.54 (s, 1H), 7.73 (s, 1H), 7.49 (d, *J* = 7.5 Hz, 2H), 7.41-7.20 (m, 7H), 7.11 (t, *J* = 7.4 Hz, 1H), 5.79 (d, *J* = 7.5 Hz, 1H), 5.19 -5.03 (m, 2H), 4.45-4.31 (m, 1H), 3.70-3.62 (m, 2H), 2.60(t, *J* = 7.5 Hz, 2H), 1.98-1.91 (m, 1H), 1.81-1.60 (m, 5H), 1.54-1.41 (m, 2H), 1.36-1.18 (m, 6H), 0.87 (t, *J* = 7.0 Hz, 3H). ^{13}C NMR (126 MHz, $CDCl_3$):

δ 205.84, 170.21, 156.75, 137.38, 135.88, 128.99, 128.60, 128.33, 127.95, 124.71, 120.16, 67.34, 55.19, 47.16, 45.34, 31.91, 31.52, 29.47, 28.66, 27.07, 22.65, 22.53, 14.06. LCMS (ESI) calcd. for $C_{27}H_{38}N_3O_3S$ $[M+H]^+$ 484.3, obsd. 484.3;

TM (91% yield) ^{1}H NMR (400 MHz, CD_3OD): δ 7.53 (d, *J* = 8.0 Hz, 2H), 7.41-7.12 (m, 7H), 7.08 (t, *J* = 7.4 Hz, 1H), 5.22-4.97 (m, 2H), 4.22 (dd, *J* = 8.8, 5.4 Hz, 1H), 3.57 (t, *J* = 7.1 Hz, 2H), 2.54 (t, *J* = 7.6 Hz, 2H), 1.90-1.79(m, 1H), 1.79-1.61 (m, 5H), 1.55-1.37 (m, 2H), 1.26 (s, 20H), 0.87 (t, *J* = 6.7 Hz, 3H). ^{13}C NMR (126 MHz, $CDCl_3$): δ 205.84, 170.18, 156.75, 137.37, 135.88, 128.99, 128.60, 128.33, 127.95, 124.71, 120.16, 67.35, 55.19, 47.21, 45.35, 31.93, 29.70, 29.67, 29.65, 29.55, 29.40, 29.37, 29.06, 27.08, 22.70, 22.65, 14.15.

LCMS (ESI) calcd. for $C_{34}H_{52}N_3O_3S$ $[M+H]^+$ 582.4, obsd. 582.4;

3. Synthesis of compound M

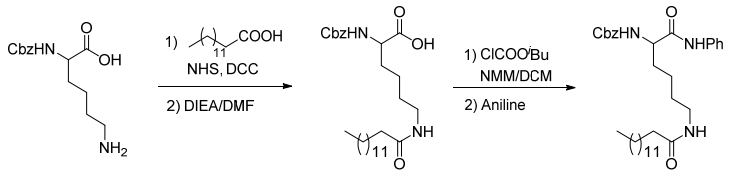

1 **6** **M**

The synthesis of compound **6** followed the method using in the synthesis of compound **4.** To a solution of compound **6** (4.9 g, 10 mmol) and *N*-methylmorpholine (1.1ml, 10 mmol) in dry dichloromethane (100 mL) at 0°C was added dropwisely iso-butylchloroformate (1.3 ml, 10 mmol). The reaction mixture was stirred 30 min at 0°C. Aniline (1.09 ml, 12 mmol) was added at 0°C and the reaction mixture was stirred overnight at rt. The solvent was removed under reduced pressure and the resulting residue was purified by silica gel chromatography (DCM/MeOH = 50:1) to afford the expected compound **M** (5.14 g, 91% yield). ^{1}H NMR (400 MHz, CD_3OD): δ 7.53 (d, *J* = 7.9 Hz, 2H), 7.40-7.13 (m, 7H), 7.08 (t, *J* = 7.4 Hz, 1H), 5.13-5.02 (m, 2H), 4.20 (dd, *J* = 8.5, 5.5 Hz, 1H), 3.15 (t, *J* = 6.7 Hz, 2H), 2.11 (t, *J* = 7.6 Hz, 2H), 1.88-1.64 (m, 2H), 1.62-1.34 (m, 6H), 1.32-1.21 (s, 20H), 0.87 (t, *J* = 7.0 Hz, 3H). ^{13}C NMR (126 MHz, DMSO-d6): δ 172.35, 171.54, 156.53, 139.43, 137.46, 129.11, 128.77, 128.22, 128.14, 123.67, 119.66, 65.87, 55.85, 38.61, 35.92, 31.98, 31.76, 29.53, 29.50, 29.48, 29.41, 29.35, 29.24, 29.18, 29.15, 25.77, 23.48, 22.56, 14.41.LCMS (ESI) calcd. for $C_{34}H_{52}N_3O_4$ $[M+H]^+$ 566.4, obsd. 566.5;

4. Synthetic Route for Biotin-TM and Biotin-M

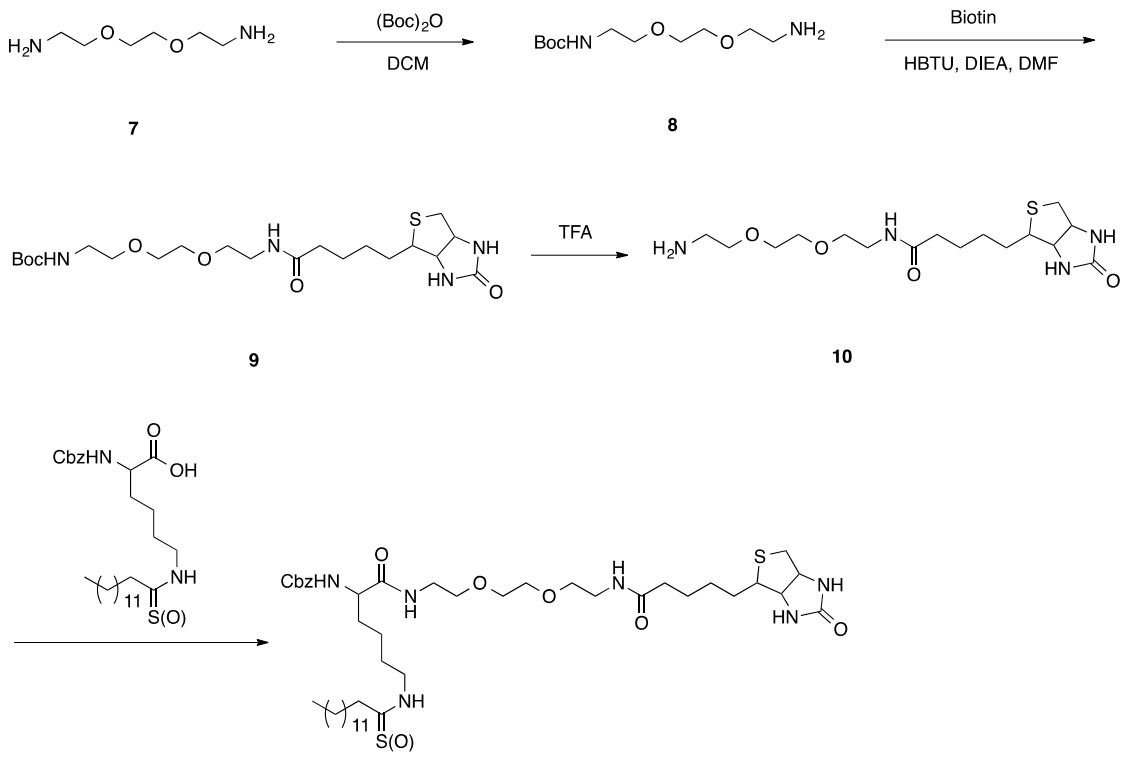

Synthesis of Compound 8. To a solution of compound **7** (14.8 g, 100 mmol) in DCM (200 mL) was added 100 mL of di-tert-butyl dicarbonate (2.18 g, 10mmol) in DCM at 0°C. The reaction mixture was allowed to warm to rt and stirred extensively overnight. The organic phase was washed with water, until all the unreacted compound **7** was extracted. After drying over Na_2SO_4 and concentration under vacuum the Boc-protected compound **8** was quantitatively obtained.

Synthesis of Compound 9. To a solution of Biotin (2.2 g, 9 mmol) and HBTU (3.41 g, 9 mmol) in DMF (30 mL) was added DIEA (3.6 mL, 20 mmol) at room temperature with stirring for 30 min. Then compound **8** was added to the resulting mixture. The reaction mixture was stirred extensively overnight. After removal of the solvents under reduced pressure, the residue was purified by flash chromatography on silica gel (DCM/MeOH = 20:1 then 10:1) to afford the expected compound **9** (3.5 g, 81% yield).

Synthesis of Compound 10. To 20 mL of TFA was added the compound **9** (2 g, 4.2 mmol) and the resulting mixture was stirred for 30 min at room temperature. After removing the solvent under vacuum the deprotected compound **10** was quantitatively obtained and used in the next step without further purification.

Synthesis of Compound Biotin-TM and Biotin-M. The synthesis followed the method using in the synthesis of **TM**. The solvent used to dissolve the compound **10** is DMF instead of DCM.

Biotin-TM (81% yield) ^{1}H NMR (500 MHz, CD_3OD): δ 7.41-7.29 (m, 5H), 5.18-5.05 (m, 2H), 4.49 (dd, *J* = 7.8, 4.8 Hz, 1H), 4.30 (dd, *J* = 7.9, 4.5 Hz, 1H), 4.10 (dd, *J* = 8.7, 5.4 Hz, 1H), 3.66-3.52 (m, 10H), 3.44 -3.34 (m, 4H), 3.21 (dt, *J* = 9.9, 5.6 Hz, 1H), 2.93 (dd, *J* = 12.7, 5.0 Hz,

1H), 2.71 (d, *J* = 12.7 Hz, 1H), 2.59 (t, *J* = 7.4 Hz, 2H), 2.22 (t, *J* = 7.4 Hz, 2H), 1.86-1.55 (m, 10H), 1.48-1.38 (m, 4H), 1.35-1.25(m, 20H), 0.91 (t, *J* = 6.9 Hz, 3H). ^{13}C NMR (126 MHz, CD_3OD): δ 205.01, 174.72, 173.54, 164.68, 156.99, 136.77, 128.10, 127.64, 127.42, 69.92, 69.21, 69.09, 66.29, 61.95, 60.21, 55.61, 55.06, 45.68, 45.16, 39.66, 38.91, 35.35, 31.68, 29.44, 29.41, 29.37, 29.33, 29.24, 29.08, 28.57, 28.37, 28.10, 26.92, 25.45, 22.95, 22.34, 13.06. LCMS (ESI) calcd. for $C_{44}H_{75}N_6O_7S_2$ $[M+H]^+$ 863.5, obsd. 863.6.

Biotin-M (83% yield)^{1}H NMR (400 MHz, CD_3OD): δ 7.39-7.22 (m, 5H), 5.10-5.04 (m, 2H), 4.46 (dd, *J* = 7.9, 4.9 Hz, 1H), 4.27 (dd, *J* = 7.8, 4.5 Hz, 1H), 4.05 (dd, *J* = 8.8, 5.3 Hz, 1H), 3.58 (s, 4H), 3.52 (q, *J* = 5.2 Hz, 4H), 3.37-3.32 (m, 4H), 3.19-3.11 (m, 3H), 2.89 (dd, *J* = 12.7, 5.0 Hz, 1H), 2.68 (d, *J* = 12.7 Hz, 1H), 2.19 (t, *J* = 7.5 Hz, 2H), 2.13(t, *J* = 7.5 Hz, 2H), 1.80-1.34 (m, 14H), 1.26 (s, 20H), 0.88 (t, *J* = 6.8 Hz, 3H). ^{13}C NMR (126 MHz, DMSO): δ 172.58, 172.50, 172.35, 163.15, 156.36, 137.49, 128.77, 128.21, 128.10, 69.98, 69.62, 69.42, 65.79, 61.48, 59.64, 55.88, 55.06, 38.97, 38.88, 38.65, 35.90, 35.55, 32.14, 31.76, 29.53, 29.49, 29.41, 29.31, 29.25, 29.18, 29.15, 28.66, 28.49, 25.78, 25.72, 23.36, 22.56, 14.43. LCMS (ESI) calcd. for $C_{44}H_{75}N_6O_8S$ $[M+H]^+$ 847.5, obsd. 847.8.

Supplemental References

Debacq-Chainiaux, F., Erusalimsky, J. D., Campisi, J., and Toussaint, O. (2009). Protocols to detect senescence-associated beta-galactosidase (SA-betagal) activity, a biomarker of senescent cells in culture and in vivo. Nat. Protoc. *4*, 1798-1806.

Du, J., Jiang, H., and Lin, H. (2009). Investigating the ADP-ribosyltransferase activity of sirtuins with NAD analogues and 32P-NAD. Biochemistry *48*, 2878-2890.

He, B., Hu, J., Zhang, X., and Lin, H. (2014). Thiomyristoyl peptides as cell-permeable Sirt6 inhibitors. Org. Biomol. Chem. *12*, 7498-7502.

Jiang, H., Khan, S., Wang, Y., Charron, G., He, B., Sebastian, C., Du, J., Kim, R., Ge, E., Mostoslavsky, R.*, et al.* (2013). SIRT6 regulates TNF-alpha secretion through hydrolysis of long-chain fatty acyl lysine. Nature *496*, 110-113.

Mabjeesh, N. J., Escuin, D., LaVallee, T. M., Pribluda, V. S., Swartz, G. M., Johnson, M. S., Willard, M. T., Zhong, H., Simons, J. W., and Giannakakou, P. (2003). 2ME2 inhibits tumor growth and angiogenesis by disrupting microtubules and dysregulating HIF. Cancer Cell *3*, 363-375.